nagra National Cooperative for the Disposal of Radioactive Waste

TECHNICAL REPORT 03-10

Time-dependent Flow and Transport Calculations for Project Opalinus Clay (Entsorgungsnachweis)

July 2004

G. Kosakowski

Paul Scherrer Institut, Villigen PSI

Hardstrasse 73, CH-5430 Wettingen/Switzerland, Telephone +41-56-437 11 11

This report was prepared on behalf of Nagra. The viewpoints presented and conclusions reached are those of the author(s) and do not necessarily represent those of Nagra.

PREFACE

The Laboratory for Waste Management of the Nuclear Energy and Safety Research Department at the Paul Scherrer Institut is performing work to develop and test models as well as to acquire specific data relevant to performance assessments of planned Swiss nuclear waste repositories. These investigations are undertaken in close co-operation with, and with the financial support of, the National Cooperative for the Disposal of Radioactive Waste (Nagra). The present report is issued simultaneously as a PSI-Bericht and a Nagra Technical Report.

ISSN 1015-2636

Abstract

This report describes two specific assessment cases used in the safety assessment for a proposed deep geological repository for spent fuel, high level waste and long-lived intermediate-level waste, sited in the Opalinus Clay of the Zürcher Weinland in northern Switzerland (Project *Entsorgungsnachweis*, NAGRA, 2002d).

In this study the influence of time dependent flow processes on the radionuclide transport in the geosphere is investigated. In the Opalinus Clay diffusion dominates the transport of radionuclides, but processes exist that can locally increase the importance of the advective transport for some time. Two important cases were investigated:

(1) glaciation-induced flow due to an additional overburden in the form of an ice shield of up to 400 m thickness and (2) fluid flow driven by tunnel convergence.

For the calculations the code FRAC3DVS (Therrien & Sudicky, 1996) was used. FRAC3DVS solves the three-dimensional flow and transport equation in porous and fractured media.

For the case of glaciation-induced flow (1) a two-dimensional reference model without glaciations was calculated. During the glaciations the geosphere release-rates are up to a factor of about 1.7 higher compared to the reference model. The influence of glaciations on the transport of cations or neutral species is less than for anions, since the importance of the advective transport for anions is higher due to the lower accessible porosity for anions. The increase in the release rates during glaciations is lower for sorbing compared to non-sorbing radionuclides. The influence of the tunnel convergence (2) on the transport of radionuclides in the geosphere is very small. Due to the higher source term the geosphere release rates are slightly higher if tunnel convergence is considered.

In addition to the two assessment cases this report investigates the applicability of the one-dimensional approximation for modelling transport through the Opalinus Clay. For the reference case of the safety assessment the model chain STMAN-PICNIC-TAME is used. In order to evaluate radionuclide release and transport, the geometry of the repository near-field/geosphere system is simplified and the Opalinus Clay is treated as a one-dimensional layer. In this study the code FRAC3DVS is used to assess the effects of the simplifications by calculating a two-dimensional model which includes both the Opalinus Clay and the SF / HLW bentonite annulus.

The one-dimensional approximation gives results similar to the geometrically more realistic FRAC3DVS model. Discrepancies introduced by the one-dimensional approximation are shown to be small and the results are always conservative compared with the FRAC3DVS calculations. This modelling exercise thus gives strong support for the applicability of the one-dimensional approximation.

Zusammenfassung

Dieser Bericht dokumentiert zwei spezifische Rechenfälle die im Rahmen der Sicherheitsanalyse eines geologischen Tiefenlagers für abgebrannte Brennelemente, hochaktive verglaste Abfälle aus der Wiederaufarbeitung abgebrannter Brennelemente und langlebige mittelaktive Abfälle im Opalinuston des potentiellen Standortgebiets im Züricher Weinlands in der Nordostschweiz, durchgeführt wurden (Projekt *Entsorgungsnachweis*, NAGRA, 2002d).

In dieser Studie wird der Einfluss von zeitabhängigen Fliessfeldern auf den Transport von Radionukliden durch die Geosphäre untersucht. Im Opalinuston dominiert generell die Diffusion den Radionuklidtransport, aber es treten auch Prozesse auf, die für eine kurze Zeit das lokale Fliessfeld und damit auch den advektiven Transport von Radionukliden verstärken können. Zwei wichtige Fälle wurden untersucht:

(1) Wasserfluss durch die Kompaktion des Opalinustons auf Grund von Vergletscherung (zusätzliche Auflast durch eine Eismächtigkeit von bis zu 400 Metern) und (2) das Auspressen von Fluiden aus den Lagerstollen durch Tunnelkonvergenz.

Für die Rechnungen wurde der Code FRAC3DVS (Therrien & Sudicky, 1996) verwendet. FRAC3DVS löst die dreidimensionalen Strömungs- und Transport-gleichungen in geklüfteten und porösen Medien.

Im Fall (1) – Wasserfluss als Folge von Vergletscherungen - wurde zuerst ein zweidimensionales Referenzmodell ohne Einfluss der Vergletscherung mit FRAC3DVS berechnet. Im Vergleich zum Referenzmodell sind während der Vergletscherungen die Geosphären-Freisetzungsraten bis zu einem Faktor von 1.7. Der Einfluss von Vergletscherung auf den Transport von Kationen und neutralen Spezies ist geringer als für Anionen, weil die Bedeutung des advektiven Transports für Anionen grösser ist. Der Anstieg der Freisetzungsraten während Vergletscherungen ist geringer für sorbierende im Vergleich zu nicht-sorbierenden Nukliden. Der Einfluss der Tunnelkonvergenz (2) auf den Radionuklidtransport in der Geosphäre ist sehr gering. Die Freisetzungraten aus der Geosphäre sind etwas höher wenn die Tunnelkonvergenz berücksichtigt wird. Dies kann als Folge eines etwas höheren Quellterms während der Phase der Tunnelkonvergenz gesehen werden.

Neben den beiden Rechenfällen wird die Anwendbarkeit des eindimensionalen Modellkonzepts für die Berechnung des Transports durch den Opalinuston untersucht. Der Referenzfall der Sicherheitsanalyse wird mit der Modellkette STMAN-PICNIC-TAME berechnet. Bei der Berechnung der Freisetzung und des Transport der Radionuklide wird die Geometrie des Nahfeldes und der Geosphäre vereinfacht wobei der Opalinuston als eindimensionaler Transportpfad behandelt wird. Um die Auswirkungen dieser Vereinfachungen abzuschätzen wurde mit Hilfe des Rechencodes FRAC3DVS in dieser Studie ein zweidimensionales Model erstellt, das den Opalinuston und den Bentonitannulus um die SF/HLW – Abfallbehälter berücksichtigt.

Die eindimensionale Näherung und das geometrisch realistischere FRAC3DVS Modell ergeben sehr ähnliche Resultate. Die Unterschiede sind nur klein und im Vergleich zu den FRAC3DVS Rechnungen sind die Resultate des eindimensionalen Modells immer konservativ. Diese Modellstudie bestätigt daher die Anwendbarkeit des eindimensionalen Modellkonzepts.

Résumé

Ce rapport donne une description de deux cas spécifiques utilisés dans le cadre de l'analyse de la sûreté radiologique à long terme d'un dépôt souterrain en profondeur, situé dans des Argiles à Opalinus du « Weinland zurichois » (Zürcher Weinland) dans le nord de la Suisse et destiné aux assemblages combustibles usés (AC), aux déchets de haute activité vitrifiés (DHA), ainsi qu'aux déchets de moyenne activité à vie longue (Projet *Entsorgungsnachweis*, NAGRA, 2002d).

Dans cette étude, l'influence des processus d'écoulement en fonction du temps sur le transport des radionucléides dans la géosphère est étudiée. Dans l'Argile à Opalinus, la diffusion est le processus contrôlant la migration des radionucléides, mais il y a des processus qui localement peuvent augmenter l'importance d'un transport par advection pendant un certain temps. Deux cas importants ont été étudiés: (1) un flux par consolidation à cause d'une glaciation (une couverture supplémentaire sous la forme d'une couche de glace avec une épaisseur atteignant jusqu'au 400 m) et (2) un flux de fluide résultant de la convergence du tunnel.

Pour les calculs, le code FRAC3DVS a été utilisé. FRAC3DVS calcule un flux en trois dimensions et trouve une solution pour l'équation de transport dans des médias poreux et fracturés.

Pour le cas d'un flux induit par la glaciation (1) un modèle de référence en deux dimensions en l`absence de glaciation a été calculé. Pendant la glaciation, les taux de relâchement dans la géosphère sont d'un facteur de 1.7 plus élevés par rapport au modèle de référence. L'influence de la glaciation sur le transport des cations et des espèces neutres est moins élevée que pour des anions, parce que l'importance d'un flux par advection est plus élevée pour des anions à cause d'une porosité plus faiblement accessible pour ces derniers. L'augmentation des taux de relâchement pendant des glaciations est plus petite pour des radionucléides sorbants comparé aux radionucléides non-sorbants. L'influence d'une convergence du tunnel (2) sur la migration des radionucléides dans la géosphère est faible. Les taux de relâchement dans la géosphère sont légèrement supérieurs dans le cas où la convergence du tunnel est considérée. Ceci est attribué aux termes de source qui sont augmentés pendant la convergence du tunnel.

Ce rapport décrit, en plus de ces deux cas, l'applicabilité d'une approximation à une dimension pour la modélisation de transport dans l'Argile à Opalinus. Pour le « scénario de référence » de lévaluation de sûreté, le modèle en chaîne STMAN-PICNIC-TAME a été utilisé. Pour évaluer le relâchement et la migration des radionucléides, la géométrie de l'interface champ proche/géosphère d'un dépôt souterrain a été simplifiée et l'Argile à Opalinus a été traitée comme une couche à une dimension. Le code FRAC3DVS a été utilisé pour évaluer les effets de cette simplification par calculation d'un modèle en deux dimensions incluant à la fois l'Argile à Opalinus et le AC/DHA annulés du bentonite.

L`approximation à une dimension donne des résultats qui sont proches d'une géométrie plus réaliste dans le modèle FRAC3DVS. Les différences introduites par l'approximation à une dimension sont petites et les résultats sont toujours conservatifs par rapport aux calculs FRAC3DVS. Cet exercice de modélisation donne ainsi un support important en faveur de l'applicabilité d'une approximation à une dimension.

Table of contents

List of Figures

Figure 30: Detail of Figure 29 for the transport of ^{129}I. Additionally the ratio of the mass flow rates out of the geosphere with and without tunnel convergence is drawn (right axis). For the release maximum, the mass flow rate for the tunnel convergence case is only 3.6 % higher than for the reference case. 50

List of Tables

1 Introduction

This report presents two specific assessment cases used in the safety assessment for a deep geological repository for spent fuel, high level waste and long-lived intermediate-level waste (Project *Entsorgungsnachweis*: NAGRA, 2002d).

The Opalinus Clay of the Zürcher Weinland in northern Switzerland has been identified as a potential host rock for a repository for spent fuel, high level waste and long-lived intermediate-level waste. The formation is about 100 m thick and is composed of highly consolidated and very low permeability claystone of Jurassic age.

In general, radionuclide transport in the Opalinus Clay formation is dominated by diffusion. On the one hand, fluid movements in the Opalinus Clay formation are hindered by the low permeability of the rock. On the other hand, long-term geological processes can locally enhance fluid flow.

In this study the influence of time dependent (transient) flow processes on the radionuclide transport in the Opalinus Clay formation are investigated. In this context two important cases were identified during the assessment process: consolidation driven flow due to glaciations (1) and the fluid flow driven by tunnel convergence (2).

(1) In the past glaciers from the Alps advanced to the north and the area of the potential repository site was covered by an ice layer of several hundred meters thickness for certain time periods. Long term transient flow processes due to loading and unloading were investigated by HORSEMAN ET AL. (1991). They concluded that, with respect to the pore pressure response during undrained loading the Opalinus Clay formation behaves more like a soil than a rock. For such a medium the build-up of an ice sheet drives fluids out of the Opalinus Clay layer, whereas the unloading drives fluid into the clay layer.

(2) It is possible that the ILW-part[1] of the repository will be affected by tunnel convergence induced by creeping of the Opalinus Clay. It is not expected that the cementitious backfill material will be compacted, but there is some uncertainty related to void volumes present in the waste containers. Corroded waste containers could be partially compacted and fluids can be driven from the tunnel into the host rock. This may enhance the advective transport of radionuclides in the geosphere.

In this study we therefore concentrate on numerical calculations of simplified scenarios of enhanced advective transport in the Opalinus Clay formation induced by tunnel convergence and glaciations. For the calculations the program FRAC3DVS (THERRIEN & SUDICKY, 1996) is used. FRAC3DVS is a numerical control volume finite-element and finite-difference code for the simulation of saturated-unsaturated flow in fractures and porous rock. Different solute transport mechanisms in both fractures and porous matrix are also directly accounted for.

The model chain STMAN for the near field, FRAC3DVS for the bentonite filling of the emplacement tunnels and the host rock (geosphere), and TAME for the biosphere was used to model the radionuclide release from the near field, migration though the host rock and distribution in the biosphere (NAGRA, 2002c). STMAN consists of three modules that run independently, and are termed SPENT for spent fuel, STRENG for

[1] LW: Long-lived intermediate-level radioactive waste

high level waste and STALLION for long-lived intermediate-level waste. In this report only the FRAC3DVS calculations are described. The results of the STMAN calculations were provided by Nagra and implemented as boundary condition in FRAC3DVS. The FRAC3DVS results, radionuclide release rates from the host rock, were delivered to Nagra for further processing with TAME.

In addition to the two assessment cases this study investigates the applicability of the one-dimensional approximation for modelling transport through the Opalinus Clay. For the reference case the model chain STMAN-PICNIC-TAME is used. In order to evaluate radionuclide release and transport, the geometry of the repository near-field/geosphere system is simplified and the Opalinus Clay is treated as a one-dimensional layer. The code FRAC3DVS is used to assess the effects of the simplifications by calculating a two-dimensional model which includes both the Opalinus Clay and the SF / HLW bentonite annulus.

In this report the utilised numerical code FRAC3DVS and the conceptual models for the geometry, boundary conditions and the considered processes will be introduced in section 2. Then, in section 3, the calculated cases, the two-dimensional reference model, and the models for glaciation induced flow and tunnel convergence are described. In section 4 the results of the calculations are presented and discussed. The last section summarizes the results.

2 Methodology

This chapter gives a description of the methodology adopted in the PSI modelling study. The simulation code FRAC3DVS used in this study is presented in the framework of the general methodology. In section 2.1 the general features of FRAC3DVS are introduced. A mathematical description of the flow and transport processes as they are implemented in FRAC3DVS is given in section 2.3. Section 2.4 deals with the theory of consolidation after Terzaghi and their connection to the time-dependent flow equation for flow in confined aquifers. The numerical treatment of the basic equations from section 2.3 within FRAC3DVS is summarized in section 2.5.

2.1 FRAC3DVS calculations: Scope and purpose

The numerical code FRAC3DVS can be used to calculate the transport of radionuclides through the geosphere. The code is described in detail in THERRIEN & SUDICKY (1996) and in THERRIEN ET AL. (1999). It solves the three-dimensional groundwater flow and solute transport equations in discretely fractured and porous media. Processes and phenomena explicitly included in FRAC3DVS are:

- Transient flow of fluids in partially- or fully-saturated porous media, in fractures and in fractured-porous media
- Advective, dispersive and diffusive transport of solutes
- Diffusion of solutes from a fracture into a limited porous rock matrix
- Linear sorption of solutes on fracture surfaces and in the rock matrix
- Radioactive decay of solutes
- Chain decay of solutes

Other flow and transport processes are included implicitly, for example through the selection of appropriate parameter values and boundary conditions.

With FRAC3DVS it is possible to calculate variable-saturated groundwater flow, but this is not used and all calculations described in this report are based on flow in a fully saturated medium.

FRAC3DVS needs as input boundary conditions the radionuclide release rates from the near-field models, and provides radionuclide release rates, which are used for the biosphere-transport modelling.

2.2 Modelling strategies

Due to its modular design, FRAC3DVS allows the use of different modelling strategies, as shown in Figure 1.

Three main model concepts are possible, **continuum models**, **discrete fractured porous-medium models** and **discrete fracture models**. The appropriate model concept for a problem depends on the model scale, the significance of inhomogeneities (geological and/or artificial), and of course on the knowledge about the system under consideration.

Continuum models are applied if it is possible to divide the inhomogeneous domain into homogeneous sub domains. This is based on the concept of the representative elementary volume (REV). The size of the homogeneous sub domains should be chosen in such a way that there are no fluctuations of the physical parameters and that it is possible to allow the inclusion of significant heterogeneities.

Discrete fracture network models can be applied if large-scale heterogeneities dominate the flow and/or transport in the domain. In this case it is not possible to approximate single connected fractures with a porous medium and the REV is larger than the model domain.

Discrete fractured porous medium models are applied if the exchange processes between fractures and matrix are important. In such hybrid models discrete fractures are placed into a porous matrix, and the matrix is implemented, e.g. for the Opalinus clay, in terms of a continuum model.

It is important to mention that for an approximation by a (normally more complex) discrete fractured porous medium model the knowledge about the real system has to be much better than for a (normally simpler) continuum model. The complexity of a model also increases the effort needed for the whole modelling process, e.g. more complex model setup, longer numerical calculations and more complicated data analysis (see Figure 1).

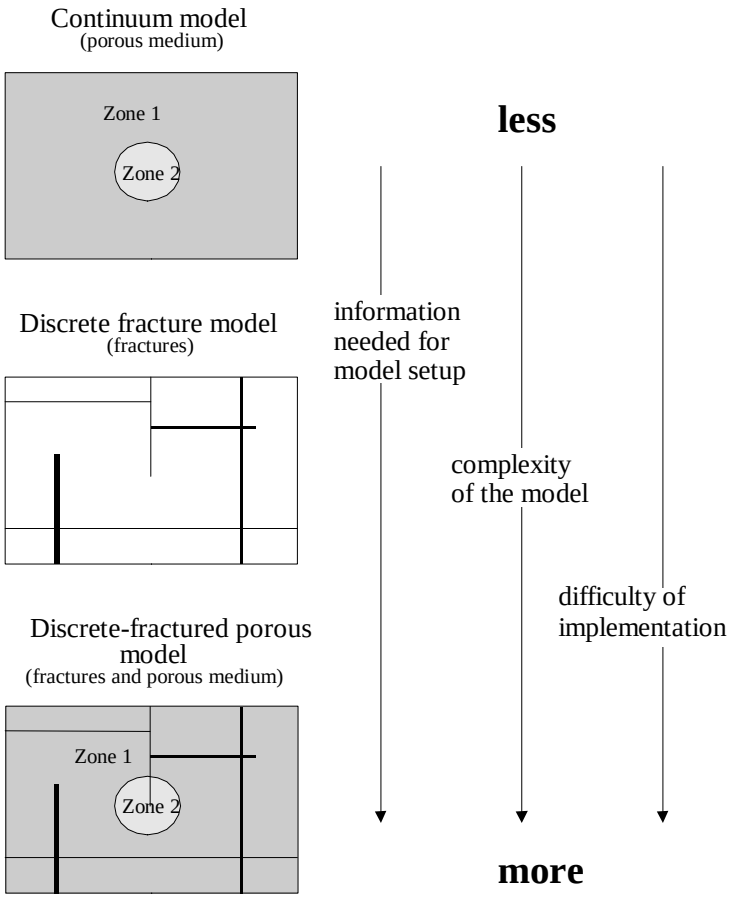

Figure 1: Modelling strategies with FRAC3DVS.

2.2.1 Phenomena included in FRAC3DVS

The relevant events and processes that are related with the far field and can be included in FRAC3DVS simulations are presented in Table 1. The features of the far field that can be calculated with FRAC3DVS are shown in Table 2. Both tables are summarized in Figure 2.

Table 1: Events and processes that can be described with FRAC3DVS.

Events and processes	**Representation in FRAC3DVS**	**Data requirements**[2]
Solutes are transported and dispersed by fluids due to hydraulic potentials and gradients in the host rock.	The three-dimensional flow equation is solved for stationary and transient boundary conditions. Based on the flow solution the three-dimensional advection-dispersion equation is solved.	Geometry of the system. Effective hydraulic conductivity [L/T]. Specific storage coefficient [1/L]. Boundary conditions: hydraulic heads [L] or volume flow rates [L^3/T]. Transversal and longitudinal dispersion lengths [L].
Solutes are transported down chemical gradients in matrix pore water and fracture-filling water.	Diffusion processes are considered at all time during model run.	Free solution diffusion coefficient [L^2/T]. Effective porosity [L^3/L^3]. Tortuosity of the rock matrix.
Solutes are retarded due to sorption onto the surface of fractures and matrix pores.	Sorption processes on fracture surfaces and in the porous matrix are implemented by the calculation of an effective retardation parameter based on a linear adsorption isotherm.	Volumetric distribution coefficient [L^3/M]. (Fracture-) Surface-based distribution coefficient [L]. Bulk density of the rock [M/L^3].
Radioactive decay in daughter nuclides takes place.	First-order radioactive decay and chain decay can be considered. The transport equation is solved for each nuclide.	First-order decay constant [1/T]. Mass fraction of a parent species transforming into a daughter species per time.
Changes in the hydraulic heads, gradients and flow rates due to uplift or subsidence (e.g. glaciation).	Time-dependent hydraulic boundary conditions mimic the effects of uplift or subsidence on the pressure field.	Time dependent boundary conditions: hydraulic heads [L] or volume flow rates [L^3/T]. Specific storage coefficient [1/L].

[2] The parameters are explained in section 2.3 and parameter values are summarized in the appendix.

Table 2: Features of the geosphere that can be included in FRAC3DVS.

Features	**Representation in FRAC3DVS**	**Data requirements**
Spatial variations of the hydraulic and transport properties of the host rock.	The host rock is divided into different regions and each region is assigned effective hydraulic and transport parameters.	Effective hydraulic and transport parameters.
An excavation-disturbed zone around the emplacement tunnels exists.	The geometry of the excavation-disturbed zone can be included in FRAC3DVS and it is possible to assign effective hydraulic and transport parameters to this zone. Cylindrical geometries of the EDZ are not the only shapes which can be implemented, more irregular shapes are possible, too.	Geometry of the excavation-disturbed zone. Effective hydraulic and transport parameters.
Possible existence of single high-conductivity features (e.g. fractures, joints, faults) and interconnected features (fracture network) within the host rock.	High-conductivity features can be considered 1) as discrete fracture planes with a constant (or variable) aperture for each plane. The hydraulic conductivity of these features can be calculated either via the cubic law or can be assigned directly. 2) as equivalent porous zones with effective hydraulic and transport parameters.	Fracture aperture [L] and/or hydraulic conductivity of the fracture [L/T]. Specific storage coefficient for a fluid-filled fracture [1/L]. Longitudinal and transversal dispersion length inside the fracture [L].

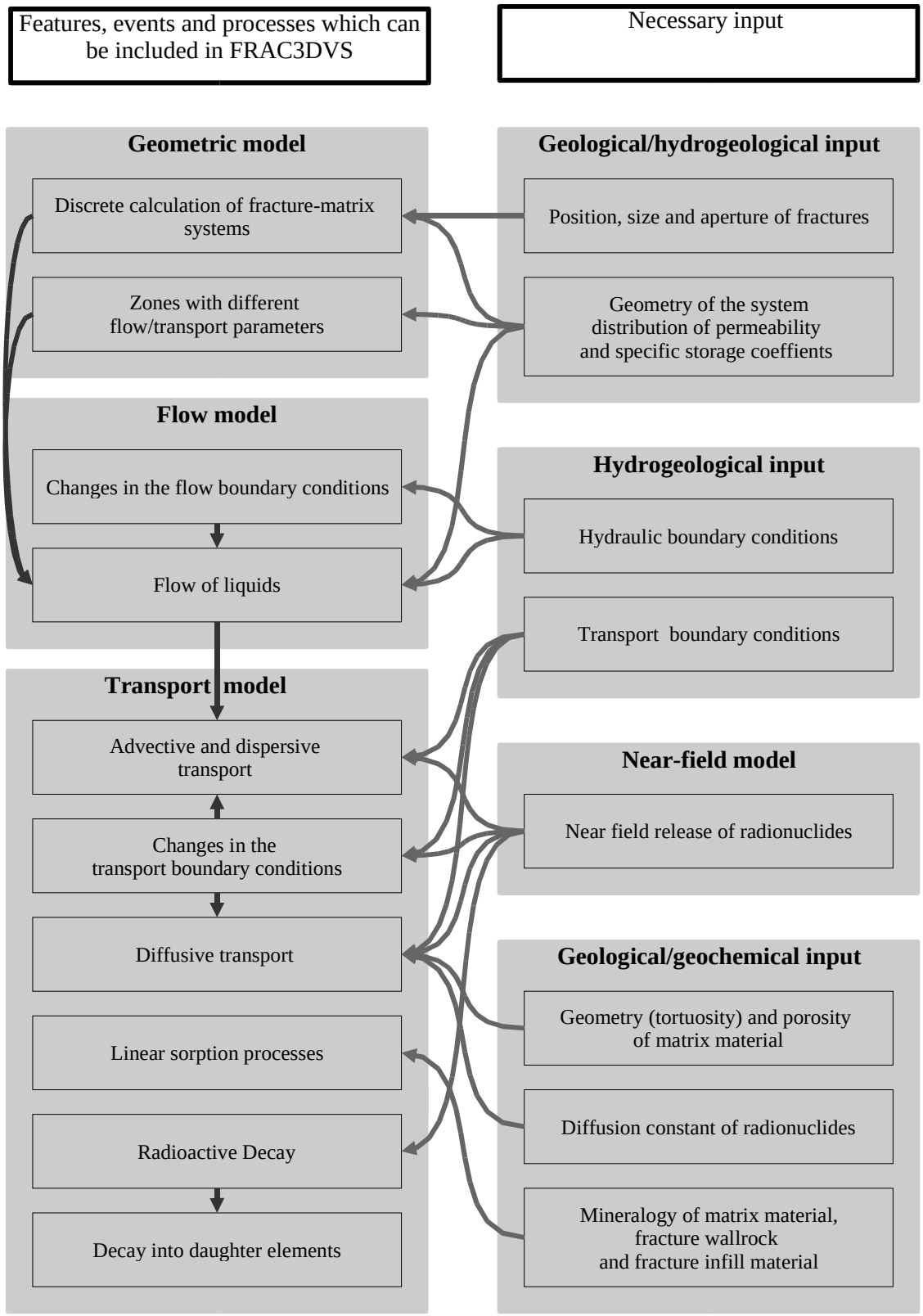

Figure 2: Input sources needed for FRAC3DVS model setup.

2.2.2 Verification

The accuracy of the FRAC3DVS code has been verified by comparing the computational results with analytical solutions (where available) and by comparison with results from other numerical codes. Table 3 summarizes the test cases.

Table 3: Test cases for the verification of the numerical code FRAC3DVS.

Case	Process, features, events	Comparison/Author
1D-consolidation driven flow in a porous medium	Time dependent hydraulic head boundary function, Time dependent fluid flow in a homogeneous medium including aquifer storativity.	Analytical solution after TERZAGHI & PECK (1948): KOSAKOWSKI (2000)
Drawdown in a 2D homogeneous aquifer	Time dependent fluid flow boundary function, time dependent fluid flow in a homogeneous porous medium including aquifer storativity.	Comparison with Theis solution: THERRIEN ET AL. (1999)
Transport in a 1D homogeneous porous medium including radioactive chain decay	Advection, dispersion, retardation and radioactive chain decay.	Analytical solution: THERRIEN ET AL. (1999)
1D diffusion dominated transport in porous media	Advection, dispersion, diffusion, and decay.	Analytical solution and numerical solutions with MCOTAC: PFINGSTEN (2000)
Transport in a single fracture including radioactive chain decay and diffusion in a porous rock matrix	Advection, dispersion, diffusion, retardation, decay in fracture. Diffusion, decay, retardation in matrix.	Analytical solution: THERRIEN ET AL. (1999)
Chain decay transport in a single fracture	Advection, dispersion, diffusion, retardation, decay in fracture. Diffusion, decay, retardation in matrix.	Numerical solutions with RANCHMD, PICNIC: PFINGSTEN (2000)
Time dependent source for transport in 1D porous medium	Time dependent source concentration, advection, dispersion.	Analytical solution: THERRIEN ET AL. (1999)
Heterogeneous 2D diffusion dominated transport	Advection, diffusion, dispersion, decay, retardation, heterogeneous distribution of hydraulic conductivities.	Numerical solution with MCOTAC: PFINGSTEN (2000)

2.3 Mathematical representation

The mathematical representation of flow and transport is based on mass balance considerations, carried out over a representative elementary volume (REV) (see e.g. BEAR, 1972). Additional assumptions are described in the previous sub-section. The idea is to replace portions of a heterogeneous (disordered) medium with a hypothetical homogeneous medium that mimics the behaviour of the heterogeneous medium. The success of such an approach is highly dependent on the scale of the problem in relation to the size and structure of the heterogeneities in the medium. If the size of the heterogeneities is much smaller than the model size, the heterogeneous medium can be replaced by a homogeneous medium with effective hydraulic and transport properties. Otherwise heterogeneities have to be included explicitly into the model (compare also section 2.2).

The following sub-sections are a simplified version of the program description by THERRIEN & SUDICKY (1996). First the basic equations for water flow in porous media and in fractures are presented. Based on their solutions the equations for the transport of solutes can be formulated. After a very short presentation of the numerical implementation of these equations, some remarks about possible modelling strategies close this section.

2.3.1 Flow in porous medium

For the calculation of flow in porous media the groundwater flow equation is used

$$\frac{\partial}{\partial x_i}\left(\mathbf{K}\frac{\partial h}{\partial x_i}\right)+q_s=S_S\frac{\partial h}{\partial t},\quad i=1,2,3\ . \tag{1}$$

The hydraulic head h [L] is defined as the elevation of the piezometric water level above a datum. q_s [L T^{-1}] is a fluid sink or source term, or volumetric rate at which fluid is added to or removed from the system per unit volume of the porous medium. S_S [L^{-1}] is the specific storage, or volume of fluid released from storage in a unit volume of the porous medium per unit decline of the head. **K** [L T^{-1}] is the hydraulic conductivity tensor. In a porous medium the hydraulic conductivity tensor is defined by the Darcy-law

$$v_{D,i}=-\mathbf{K}\frac{\partial h}{\partial x_i},\quad i=1,2,3\ . \tag{2}$$

The components of the Darcy-flux $v_{D,i}$ [L T^{-1}] are a discharge per unit bulk area of the porous medium. Normally it is possible to choose a coordinate system in such a way that the axes are pointing in the same directions as the main components of the hydraulic conductivity tensor. This makes all components of the conductivity tensor, except the principal components. equal to zero

The seepage or average water velocity v_f [L T^{-1}] is defined by dividing the Darcy-flux by the flow (kinematic) porosity ε_f:

$$v_{f,i}=\frac{v_{Di}}{\varepsilon_f},\quad i=1,2,3\ . \tag{3}$$

The average water velocity is not the true microscopic fluid velocity in the matrix, but the apparent velocity in terms of linear distance along the exterior of the porous medium.

2.3.2 Transport in porous medium

In order to describe transport in discretely fractured-porous medium, two transport equations are needed, one for the porous medium and one for the fractures.

Three-dimensional transport in a porous medium is described by the following equation:

$$\varepsilon_p R_p \frac{\partial c}{\partial t} + v_{Di} \frac{\partial c}{\partial x_i} - \frac{\partial}{\partial x_i}\left(\varepsilon_p \mathbf{D}_h \frac{\partial c}{\partial x_j} \right) + \varepsilon_p R_p \lambda c + \Omega_s = 0, \quad i, j = 1,2,3 \ . \qquad (4)$$

$c=c(x_i,t)$ [M L^{-3}] is the solute concentration, $\mathbf{D}_h$ [L^2 T^{-1}] is the hydrodynamic dispersion tensor, ε_p [-] is the matrix porosity and λ [T^{-1}] is a first-order (radioactive) decay constant. Ω_s [M L^{-3} T^{-1}] is a general source or sink term representing an addition or a loss of mass. This term includes the addition of mass by chain decay for a specific nuclide.

The retardation factor for a porous medium R_p is given by

$$R_p = 1 + \frac{\rho_p}{\varepsilon_p} K_d \ . \qquad (5)$$

ρ_p [M L^{-3}] is the dry bulk density of the rock and K_d [L^3 M] is the mass-based sorption equilibrium distribution coefficient in terms of a linear adsorption isotherm.

The components of the hydrodynamic dispersion tensor $D_{h,I,j}$ are given by:

$$D_{h,i,j} = (\alpha_L - \alpha_T) \frac{v_{f,i} v_{f,j}}{|v_f|} + \alpha_T |v_f| \delta_{ij} + \varepsilon_p \tau D_w \delta_{ij}, \quad i, j = 1,2,3 \ . \qquad (6)$$

α_l [L] and α_t [L] are the longitudinal and transverse dispersion length, respectively. $|v_f|$ is the magnitude of the seepage velocity and $v_{f,i}$ are the components of the seepage velocity vector, τ [-] is the matrix tortuosity, D_w [L^2 T^{-1}] is the diffusion coefficient in water, and δ_{ij} is the Kronecker delta.

The transport Equation 4 for porous media is coupled via the Darcy Equation 2 to the flow Equation 1.

2.3.3 Flow in fractures

The fractures are idealized as two-dimensional parallel plates. This implies that the hydraulic head is uniform across the fracture width. It is now possible to formulate the flow equation for fractures in analogy to Equation 1:

$$\frac{\partial}{\partial x_i}\left(\mathbf{K} \frac{\partial h}{\partial x_i} \right) - q_{n|I^-} + q_{n|I^+} + q_s = S_{Sf} \frac{\partial h}{\partial t}, \quad i = 1,2 \ . \qquad (7)$$

Equation 1 and 7 are linked via the fluid leakage fluxes $q_{n|I^-}$ [L T^{-1}] and $q_{n|I^+}$ [L T^{-1}] across the two fracture surfaces I^- and I^+, respectively, of a fracture. Here we assume that there is no pressure discontinuity at the matrix-fracture interface. The hydraulic head at the matrix side equals the hydraulic head at the fracture side for all fracture surfaces.

S_{sf} [L^{-1}] is the specific storage coefficient for the fractures. Because it is assumed here that the fractures are not deformable and completely filled with fluid, there is no contribution to the storage term from the fracture compressibility. Thus the storage term is related to the fluid compressibility β_f [M^{-1} L T^2] according to:

$$S_{Sf} = \rho_f g \beta_f \quad . \tag{8}$$

Here g (9.81ms^{-1}) is the gravitational acceleration and ρ_f [M L^{-3}] the fluid density.

In the case of two-dimensional laminar flow between smooth walls with constant aperture 2b [L] it is possible to derive the law of Hagen-Poiseuille (often called cubic law) from the Navier-Stokes equations. The specific mass flow rate v_F [L T^{-1}] between parallel plates, which is equivalent to the Darcy-velocity, and which in case of open fractures is also equal to an average water velocity, can be expressed as:

$$v_{F,i} = \frac{-\rho_f g (2b)^2}{12\mu_f} \frac{\partial h}{\partial x_i}, \quad i = 1,2 \quad . \tag{9}$$

μ_f [M L^{-1} T^{-1}] is the dynamic viscosity of the fluid. For Equation 9 it is possible to define a hydraulic fracture conductivity tensor in analogy to the Darcy-law. In FRAC3DVS it is assumed that fractures are homogeneous and isotropic, therefore the hydraulic conductivity tensor is reduced to a scalar fracture conductivity K_F:

$$K_F = \frac{\rho_f g (2b)^2}{12\mu_f} \quad . \tag{10}$$

2.3.4 Transport in fractures

In analogy to Equation 4 a two-dimensional transport equation for the fractures can be formulated:

$$R_f \frac{\partial c}{\partial t} + v_{Fi} \frac{\partial c}{\partial x_i} - \frac{\partial}{\partial x_i}\left(\mathbf{D}_h \frac{\partial c}{\partial x_j} \right) + R_f \lambda c - \Omega_{n|I^-} + \Omega_{n|I^+} + \Omega_S = 0, \quad i, j = 1,2 \quad . \tag{11}$$

c=c(x_i,t) [M L^{-3}] is the solute concentration in the fracture. $\mathbf{D}_h$ [L^2 T] is the two-dimensional hydrodynamic dispersion tensor of the fracture. The components can be derived from Equation 6 by inserting the fluxes and dispersivities from the fracture and setting the fracture porosity to unity. (We do not need a special porosity term, because the fracture is open and fully saturated with water.) The terms with $\Omega_{n|I+}$ [M L^{-3} T^{-1}] and $\Omega_{n|I-}$ [M L^{-3} T^{-1}] represent advective-dispersive losses of solute mass across the surfaces I^- and I^+, respectively, of the fracture due to fluid leakage and hydrodynamic dispersion. Ω_S [M L^{-3} T^{-1}] is a general source or sink term representing an addition or a loss of mass. This term includes the addition of mass by chain decay for a specific nuclide. The retardation factor R_f [-] in the fracture is defined as

$$R_f = 1 + \frac{2K_a}{2b} \quad . \tag{12}$$

K_a [L] is a fracture-surface-based sorption equilibrium distribution coefficient in terms of a linear adsorption isotherm.

The transport Equation 11 for fractures is coupled to the flow Equation 7 for fractures via the fluid velocity in Equation 9.

2.4 Consolidation induced flow

In this study we follow the approach described e.g. by DE MARSILY (1986) and apply Terzaghi's theory of consolidation.

2.4.1 Theory of consolidation after Terzaghi

Terzaghi's theory is commonly used for the description of consolidation and compaction processes in saturated low-permeability soils (e.g. clay) due to extended load acting on such a medium.

The deformation of a finite volume of porous medium involves the compressible behaviour of both the solid matrix and the pores. Changes in the volume can be induced by changes in the internal fluid pressure *p* or an externally imposed stress σ. We consider a horizontal plane of area *A* embedded within a saturated porous media. Any changes in the load on *A* should be essentially one-dimensional and vertical. The total load on A consists of the weight *W* of rock, soil, water, and atmosphere overlying this plane. The total stress on σ on *A* is therefore equal to *W*/*A*. The plane A intersects both the solid matrix and the pores. In a static case the total stress must be balanced by interparticle stresses and fluid pressure. Terzaghi uses the term effective stress to describe the stress that is only transmitted in the solid phase as opposed to the pressure *p* of the fluid that is filling the pores. The total stress σ is therefore composed of the effective stress σ_e and the fluid pressure: $\sigma = \sigma_e + p$. Then, changes in the effective stress, which lead to changes in porosity, can be induced by altering either the total stress or the fluid pressure, or both.

The phenomenon of consolidation is associated with the outflow of interstitial water contained in the medium (soil, rock, clay). The load applied on the medium, which in case of glaciation is the additional load of an ice sheet, is absorbed by the solid phase (increase in effective stress) and partly by the interstitial water (increase in fluid pressure). During consolidation the external load, as well as the resulting total stress remains constant. At the beginning of the loading the excess load is completely absorbed by the pressure *p*. The increase in pressure starts a transient outflow of interstitial water and the load is gradually transformed into increased effective stress σ_e until the system is equilibrated again. The loss of fluid allows the consolidation.

Terzaghi's theory of consolidation assumes that:

- The outflow of the interstitial water obeys Darcy's law.
- The hydraulic conductivity of the medium does not vary during the consolidation process.
- The water and the solid elements in the medium (soil, rock, clay) matrix are incompressible; compression then means decrease in porosity.

- The compressibility of the medium is elastic. There is a linear relation between the effective compression stress and the decrease in soil volume (volume of water released)[3].

The basic differential equation for the 1D consolidation theory is (e.g. DE MARSILY, 1986, p. 97):

$$\nabla^2 p = \frac{\left(1-\varepsilon_p\right)\alpha\rho_f g}{K}\frac{\partial p}{\partial t} \tag{13}$$

α is the compressibility coefficient [L T^2 M^{-1}]

p is the pressure [M L T^{-1}]

ε_p is the total porosity (volume of the pores divided by the total volume of the solid phase and the pores) [-]

ρ_f is the fluid density [M L^{-3}]

g is the gravitational acceleration [L T^{-2}]

K is the hydraulic conductivity [L T^{-1}]

t is the time [T]

The coefficient C_V

$$C_v = \frac{\left(1-\varepsilon_p\right)\alpha\rho_f g}{K}. \tag{14}$$

is called consolidation coefficient [L^{-2} T]. The factor (1-ε_p) can be disregarded if it is close to 1.

H is introduced as the half thickness of the (Opalinus) clay layer (compare Figure 3) and a dimensionless time T_v is defined:

$$T_v = \frac{C_v t}{H^2}. \tag{15}$$

TERZAGHI & PECK (1948) give a one-dimensional analytical solution (equal to the standard solution for a diffusion/conduction problem) for the evolution of the pressure field $p(z,t)$ with the depth z and over the time t. The pressure change is described by a step function $\Delta p(z,t)$. At t=0 the initial pore pressure p_0 applies onto the whole domain; for t>0 the pressure at the boundaries (z=0 and z=2H) equals zero.

$$p(z,t) = \frac{4p_0}{\pi}\sum_{n=0}^{\infty}\frac{1}{2m+1}\sin\frac{(2m+1)\pi z}{2H}\exp\frac{-(2m+1)^2\pi^2 T_v}{4} \tag{16}$$

A solution for the Darcy flux $v_D(z,t)$ in a medium with a hydraulic conductivity K_z in z-direction is derived from Equation 16 and Darcy's law.

---

[3] DE MARSILY (1986) points out (in section 5.3) that this assumption is only an approximation of reality.

$$v_D(z,t) = -K_z \frac{\partial h(z,t)}{\partial z} = -\frac{2h_0 K_z}{H} \sum_{m=0}^{\infty} \cos\left(\frac{(2m+1)\pi z}{2H}\right) \exp\left(\frac{-(2m+1)^2 \pi^2 T_v}{4}\right) \qquad (17)$$

In the last equation the pressure p is already replaced by the hydraulic head h, the elevation of the piezometric water level above the datum z_0:

$$h = \frac{p}{g\rho_f} + z_0 \,. \qquad (18)$$

Figure 3 shows an example for the evolution of the hydraulic head and the Darcy flux over the depth z with time. For early times the Darcy flux at the boundaries is very high, whereas in the centre of the domain no water movement occurs. With increasing time the flow field moves to the interior of the domain. At the same time the hydraulic gradients and the Darcy Flux decrease. A more detailed analysis of the time dependent flow behaviour for such a system is presented in Section 4.2.1.

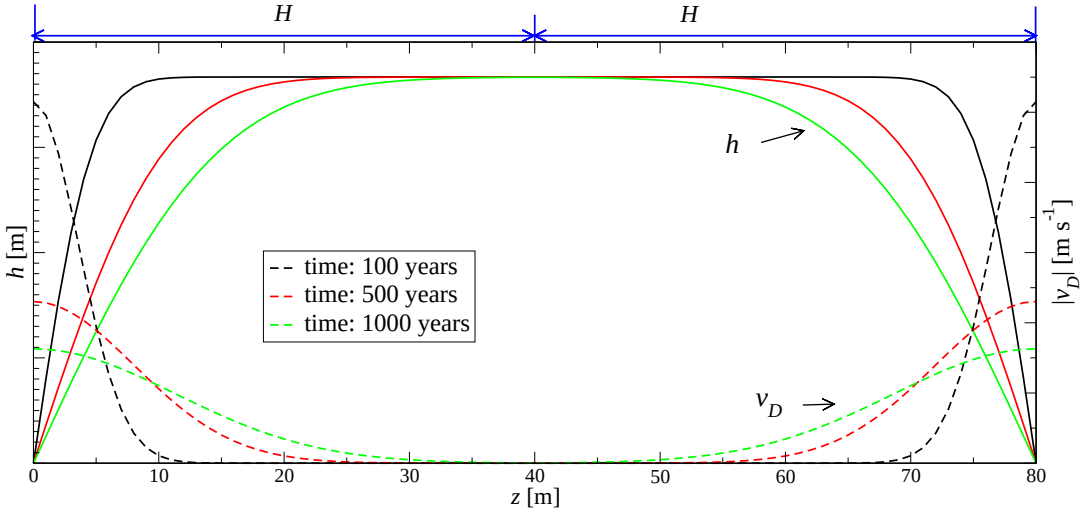

Figure 3: Example for the evolution of the head field $h(z,t)$ (solid lines) and the Darcy flux $v_D(z,t)$ (dashed line) over the depth z for three different times.

2.4.2 Flow in a confined aquifer

We repeat the basic flow Equation 1 for confined aquifers

$$\frac{\partial}{\partial x_i}\left(\mathbf{K}\frac{\partial h}{\partial x_i}\right) + q_s = S_S \frac{\partial h}{\partial t}, \quad i = 1,2,3. \qquad (19)$$

This equation is formally identical to the basic flow equation in an unconfined aquifer (S_S is replaced by the specific yield ω_d).

For the approximation of Equation 19 with Equation 13 and we need the definition of the specific storage coefficient S_S:

$$S_S = \rho_f \varepsilon_p g\left(\beta_l - \beta_s + \alpha/\varepsilon_p\right). \qquad (20)$$

β_l is the compressibility of the fluid [Pa^{-1}] and β_s the compressibility of the rock matrix [Pa^{-1}].

It is possible to simplify Equation 20 by assuming that the change in the water and the solid elements is negligible and that therefore the porosity of our medium is not changing. These are the basic assumptions also used within Terzaghi's theory of consolidation (section 2.4.1).

$$S_S = \rho_f g \alpha \tag{21}$$

If we have no additional sources or sinks (q_S=0) and the hydraulic conductivity is a scalar quantity, then our simplified definition of the specific storage coefficient is the direct link between the basic equation of Terzaghi's theory (Equation 16) and the flow equation used in FRAC3DVS (Equation 1).

2.5 Numerical implementation

The detailed description of the numerical implementation in FRAC3DVS can be found in THERRIEN & SUDICKY (1996). Here we only give a summary of the implementation and some more information, which are important for the calculations of radionuclide transport in discretely fractured porous media.

2.5.1 Solution of flow equation

The solution of the coupled flow and transport equations is based on the control volume finite-element approach (sometimes also called finite volume approach). In this method the volume of the domain, or area of the fracture domain, is discretized by a numerical grid. Around each node a control volume is defined. The differential equations are solved by direct calculation of the fluxes through each control volume. This procedure ensures fluid conservation both locally and globally.

The discretized equations presented in THERRIEN & SUDICKY (1996) are independent of the choice of the element type. Implemented are (rectangular) prism elements for the matrix and rectangular elements for the fractures. These element types produce a regular mesh, which does not allow the discretization of complex geometries. As an alternative for complex domains, tetrahedral elements for the matrix and triangular elements for the fractures can be used. It is not possible to mix both element types. Examples for possible meshing strategies are presented in Figure 4.

Additionally a finite difference formulation is implemented in the code. It can be only used with regular grids and yields similar results to the finite volume formulation. On the one hand the finite difference formulation needs four times more memory than the finite volume formulation to solve the assembled coefficient matrix, on the other hand experience indicates a fourfold increase in required CPU time to solve such a system.

A variable time-stepping procedure has been incorporated in the solution procedure for transient flow problems. After obtaining the solution at time level *I*, the next time step is selected according to:

$$\Delta t^{I+1} = \frac{h^*}{\max\left|h_i^{I+1} - h_i^I\right|}, i = 1,2,...,n \tag{22}$$

h^* is the maximum change in hydraulic head allowed during a single time step, n the number of nodes, h_i^I the head at a certain node i during time step I and h_i^{I+1} the head at a certain node i during time step I+1. To eliminate an unnecessary reduction in the time step size for the case that the range in the head function becomes very small, a lower limit for the head change can be defined.

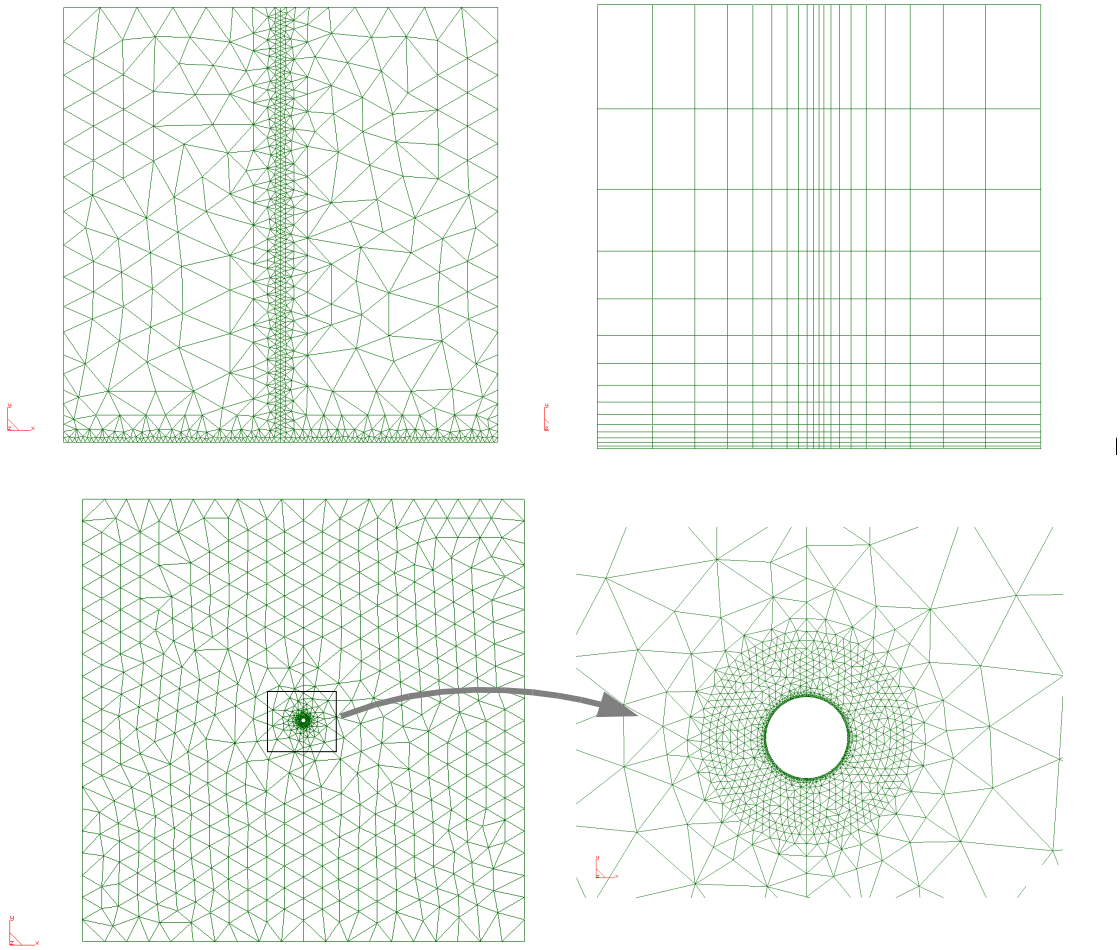

Figure 4: Possible discretizations of a model domain. Shown are 2D-slices through the 3D-model domain. Triangles are upper faces of prisms and quadrilaterals are faces of hexahedral elements. Upper row: Two possibilities for mesh refinement along a vertical fracture in the middle of the domain with triangles (left) and quadrilaterals (right). The lower boundary is refined too, because this is the location of a first-type boundary for flow and transport. Lower row: Mesh refinement around a central circular source zone.

2.5.2 Solution of the transport equation

The transport equation is solved in a similar way to the flow equation. The types of elements used for transport are identical to those used for the flow problem. There are no explicit (solute) mass exchange terms formulated, because the two-dimensional elements representing the fractures are superposed on the faces of three-dimensional matrix elements and share the same nodes.

Again it is possible to use a control volume finite element approach or a finite difference approach to solve the transport equation. Both methods give the same results for the test cases.

The variable time stepping procedure described in section 2.5.1 is also realized in a similar way for the solution of the transport problem. After obtaining the solution at time level *I*, the next time step is selected according to:

$$\Delta t^{I+1} = \frac{C^*}{\max\left|C_i^{I+1} - C_i^I\right|}, i = 1,2,...,n \qquad (23)$$

C^* is the maximum change in hydraulic head allowed during a single time step, n the number of nodes, C_i^I the concentration at a certain node i during time step I and C_i^{I+1} the concentration at the same node i during time step I+1. To eliminate unnecessary reduction in time step for the case that the range in the head function becomes very small, a lower limit for the head change can be defined.

It is possible to combine both time stepping procedures, for the flow solution and for the transport solution. From the two estimated time steps the smaller one is used for both solutions.

2.5.3 Boundary conditions

FRAC3DVS supports two types of flow boundary conditions:

- Dirichlet (first-type) boundary conditions are implemented by assigning hydraulic heads h to appropriate nodes. It is possible to assign time-variable heads

$$h = f(x_j, t), \quad j = 1,2,3 \ . \qquad (24)$$

- Neumann (second-type) boundary conditions are implemented by assigning fluid fluxes normal to the boundary.

$$K_i \frac{\partial h}{\partial x_i} = q_i = g_i(x_j, t), \quad i, j = 1,2,3 \ . \qquad (25)$$

$g_i(x_j,t)$ is a given arbitrary function representing the dispersive flux normal to the boundary.

FRAC3DVS supports three types of transport boundary conditions:

- Dirichlet (first-type) boundary conditions are implemented by assigning a concentration to the appropriate nodes. It is possible to assign time-variable concentrations.

$$c = f(x_j, t), \quad j = 1,2,3 \ . \tag{26}$$

- Neumann (second-type) boundary conditions are implemented by assigning mass fluxes to selected nodes.

$$\Omega_S = g(x_j, t), \quad j = 1,2,3 \ . \tag{27}$$

$g(x_j,t)$ is a given arbitrary function representing the mass flux for a domain.

- Cauchy (third-type) boundary conditions are implemented by assigning mixed concentration and flux values to the selected faces. Normally the mass fluxes are calculated by FRAC3DVS from the flow solution. Only positive fluxes (i.e. into the domain) are possible.

$$-\mathbf{D}\frac{\partial c}{\partial x_i} + c\frac{v_{Di}}{\varepsilon_p} = k_i(x_j, t), \quad i, j = 1,2,3 \ . \tag{28}$$

3 Model cases

This section summarizes the conceptualisation of the real geological system into the numerical models. The basic model assumptions are summarized in the section 3.1 and 3.2. The three model cases: the two-dimensional reference model, glaciation induced flow and flow driven by tunnel convergence, are presented in sections 3.3 to 3.5.

In order to evaluate radionuclide release and transport, the geometry of the repository near-field / geosphere system has to be simplified. The purpose of the first calculation case is to assess whether the simplifications used can have significant effects on calculated releases.

The second case, glaciation induced flow, investigates the influence of loading/unloading cycles due to glaciations on the transport of radionuclides. Calculations are based on the two-dimensional reference conceptualisation.

The third case, tunnel convergence induced flow, is based on a one-dimensional conceptualisation and cannot be compared directly to the two-dimensional calculations.

3.1 Overview

In the conceptualisation, the likely/expected broad evolutionary path of the disposal system is followed as in the Reference Conceptualisation (NAGRA, 2002c). It differs from the Reference Conceptualisation, however, in that compaction and decompaction of the Opalinus Clay due to glacial loading and unloading, and the resulting flow of water out of and into the Opalinus Clay, is taken into account in evaluating the transport of radionuclides through the host rock. In the Reference Conceptualisation, advection is assumed to be driven solely by the currently observed pressure difference between the lower and upper confining units, directed upwards. The conceptualisations "glacially-induced flow in the Opalinus Clay" and ”tunnel convergence“ are investigated in order to test the assumption of the Reference Conceptualisation that glacial cycling has a minor effect on overall radionuclide transport.

3.2 Basic model concept and key model assumptions

The host rock consists of the Opalinus Clay and the Murchisonae Beds in Opalinus Clay facies (although, throughout this report, the term “Opalinus Clay” is used in preference to “host rock”, and is taken to include the Murchisonae Beds). It is assumed that its transport-relevant properties are constant in space and time. In particular, uplift and erosion are assumed to have negligible effects on the hydraulic properties of the host rock over the time period of interest, and it is assumed that the host rock contains no discontinuities with significant transmissivities. Furthermore, it is assumed that no radionuclides are transported along the tunnels, ramp and shaft, or their associated excavation-disturbed zones (EDZs). In effect, the transport-relevant properties of the backfilled and sealed tunnels, ramp and shaft are not distinguished from those of the surrounding host rock. A conceptual model of the resulting geosphere transport paths is shown in Figure 5.

It is assumed that solubility limits are never exceeded within the host rock, so that radionuclides are present either in solution or as sorbed phases, but not as precipitated phases. Dissolved radionuclides are transported by diffusion and advection, with mechanical dispersion[4]. Advection is described using Darcy's law and is driven by the currently observed pressure difference between the small aquifers in the lower and upper confining units (Sandsteinkeuper, Wedelsandstein). For the reference model and the case of tunnel convergence glacial cycling is assumed to have negligible effects on advective transport. Diffusion is described using Fick's laws. Dispersion is neglected. Transport is retarded by linear, reversible, equilibrium sorption, described by an element-dependent sorption coefficient (K_d). Some radionuclides are subject to anion exclusion that affects their diffusion coefficients and the effective porosity that they see. Gas-mediated transport is assumed to be negligible. Any colloids are assumed to be immobile in the host rock and are, therefore, neglected.

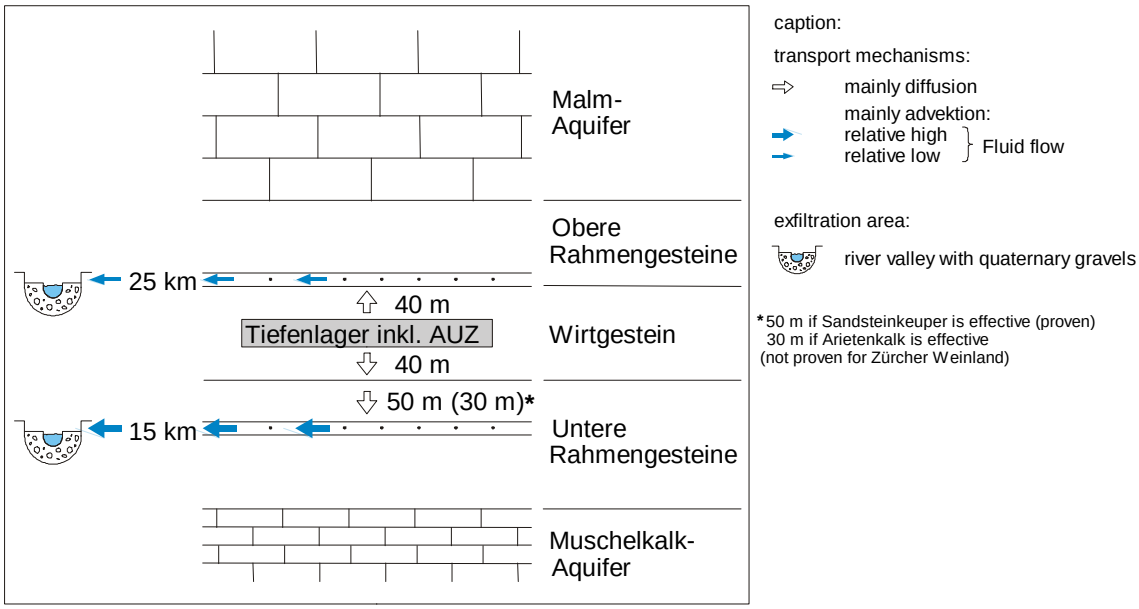

Figure 5: Conceptual transport paths in the geosphere (after NAGRA 2002a).

Table 4 summarizes the above key model assumptions employed in the cases described in this report, and explains their justification in terms, e.g., of conservatism, supporting calculations and experimental evidence.

[4] Although heterogeneity is not considered explicitly, the mechanical dispersion that is assumed to occur during transport may be considered to arise, in part, from such heterogeneity. The combination of the processes of diffusion and mechanical dispersion is sometimes termed "hydrodynamic dispersion".

Table 4: Some key model assumptions applied in this study.

Key model assumptions	Justification
The geometry of the hydraulic/transport problem can be simplified to a 2D-problem.	In the scale of the geosphere model the emplacement tunnels can be described as line sources (long cylinders) for the radionuclides. Because of the cylindrical geometry, transport can be simplified to transport in a plane normal to the extension of the tunnel.
The geometry of the system does not change over the period of assessment.	Changes in the thickness of the Opalinus Clay layer due to consolidation processes are small compared to the overall thickness of the layer, because the layer is already highly consolidated. Deformation of the source zone (emplacement tunnel) is small compared to the thickness of Opalinus Clay layer and the transport distances.
Flow in the Opalinus Clay is described by Darcy's law and flow is laminar.	There are indications for a lower limit for the validity of the Darcy law in case of sediments with very fine pores below $3\text{-}8 \cdot 10^{-6}$ m diameter. The current state of the scientific discussion does not allow the reliable formulation of flow laws for the Opalinus Clay. (see page 40, LANGGUTH & VOIGT, 1980; pages 8-9 SCHNEIDER & GÖTTNER, 1991; NAGRA, 2002c). However it is clear that the Darcy law gives an upper limit for the flow velocities and is therefore used as a conservative approximation of the flow velocities. Non-laminar flow characterized by a Reynolds number greater than 1-10 occurs in nature mainly in karst aquifers. Non-laminar flow occurs mainly in artificial flow fields in the vicinity of pumping wells or for special flow geometries (e.g. geothermal circulation systems). Both situations do not occur in the Opalinus clay. Non-laminar or turbulent flow will lead to lower flow velocities than laminar flow for the same hydraulic gradient. For the purpose of a safety assessment the conservative approach of laminar flow should be used.
Hydraulic and transport material properties of the Opalinus Clay do not change over the period of assessment.	For scenarios with changing parameters models with constant extreme values can be used for conservative estimates of the radionuclide transport.
Opalinus Clay is fully saturated with water.	The undisturbed Opalinus Clay layer is fully saturated. During excavation of the tunnels the surrounding rock will be partially drained. After deposition of the canisters and filling of the surrounding space with bentonite, the whole system will be saturated again. In case of gas production due to corrosion of the steel containers, it is assumed that the gas is dissipated by aqueous diffusion. If other processes of gas transport (e.g. mechanical opening (fracturing) of high conductivity pathways due to high gas pressures) are relevant, FRAC3DVS cannot be used.
It is possible to describe the Opalinus Clay layer with effective hydraulic and transport parameters.	Heterogeneities of the Opalinus Clay are small compared to model scale. This allows the usage of effective hydraulic and transport parameters. This assumption is based on the commonly used and accepted theory of representative elementary volumes (see e.g. BEAR, 1972). Large scale heterogeneities, e.g. the bentonite filling of the emplacement tunnels, are considered as discrete features in the models.
Sorption is linear, instantaneous, concentration dependent and reversible.	Radionuclide migration is expected to be slow compared to sorption kinetics. Sorption constants can be selected conservatively to account for any non-linearity. The assumption of reversibility is conservative.

3.3 CASE 1: The applicability of the one-dimensional approximation for modelling transport through the Opalinus Clay

For model chain calculations using the STMAN suite of codes and PICNIC, as well as for the barrier efficiency models described in Section 9.3 of NAGRA (2002c), the Opalinus Clay is treated as a one-dimensional layer. Releases from the bentonite surrounding the SF[5] / HLW[6] packages and from the ILW[7] cementitious region occur along the lower boundary of this layer and releases across the top boundary are evaluated. The bentonite surrounding the SF / HLW packages is treated as a homogeneous annular cylinder.

This geometrical simplification means, in effect, that the only transport path that is explicitly considered through the Opalinus Clay is one that starts at the upper most point of the bentonite annulus and extends for 40 m vertically upwards to the top boundary of the Opalinus Clay. In reality, the vertical transport distance varies slightly according to the point of release from the bentonite annulus. It should also be noted that perturbations to groundwater flow in the Opalinus Clay caused by the presence of the repository near field are neglected when carrying out the geometrical simplification. Furthermore, in cases where diffusive transport is dominating over advective transport, radionuclides will migrate downwards, even if the hydraulic gradient drives advective transport in the opposite direction, and will be released from the lower boundary of the Opalinus Clay.

Since the models are required to evaluate releases that are spatially integrated in the horizontal plane, the neglect of horizontal diffusion and transverse dispersion is unimportant for the release rates.

The code FRAC3DVS is used to assess the effects of the simplifications described above. FRAC3DVS is applied over the two-dimensional domain illustrated in Figure 6, which includes both the Opalinus Clay and the SF / HLW bentonite annulus. FRAC3DVS is not used in this way to model the assessment cases because it cannot take account of solubility limits, which are important for many safety-relevant radionuclides.

The code SPENT (a member of the STMAN suite of codes used to model near field release and transport in the case of spent fuel) is used to calculate radionuclide release rates of some example radionuclides at the inner boundary of the FRAC3DVS model domain, which corresponds approximately to the canister outer surface[8]. The resulting release rates across the boundaries *AA'* and *BB'* (Figure 6) are evaluated as functions of time using FRAC3DVS and summed together. The investigated radionuclides are not expected to reach their solubility limits anywhere within the modelled system.

In the Reference Case, SPENT is used to calculate radionuclide release rates at the outer boundary of the bentonite annulus, and, by applying the one-dimensional approximation, PICNIC is used to evaluate the release rates from the Opalinus Clay. A

---

5 Spent fuel

6 High-level radioactive waste

7 Long-lived intermediate-level radioactive waste

8 In order to apply FRAC3DVS to this problem, radionuclides are, in fact, released at a small distance outside the canister and inside the bentonite annulus (Boundary F in Figure 8).

comparison of results calculated using FRAC3DVS and PICNIC gives an indication of the magnitude of the effects of the one-dimensional approximation.

For the calculation of transport through the buffer, the geometry of the system is simplified in such a way that only two-dimensional transport is considered, i.e. the axial diffusion of radionuclides into the buffer separating the canisters is conservatively neglected. The release of radionuclides from the buffer surrounding the SF and HLW is thus calculated as if the waste forms were arranged end-to-end in a continuous cylinder, as illustrated in Figure 7.

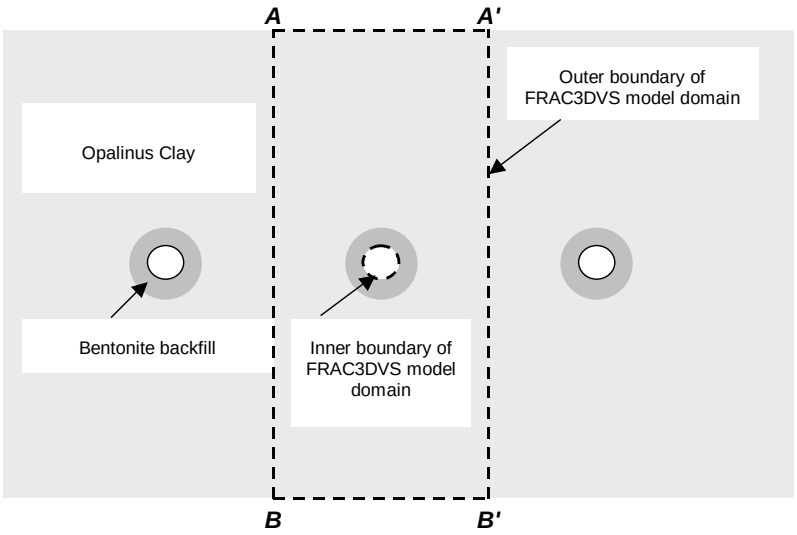

Figure 6: The two-dimensional domain modelled using FRAC3DVS (from NAGRA, 2002c).

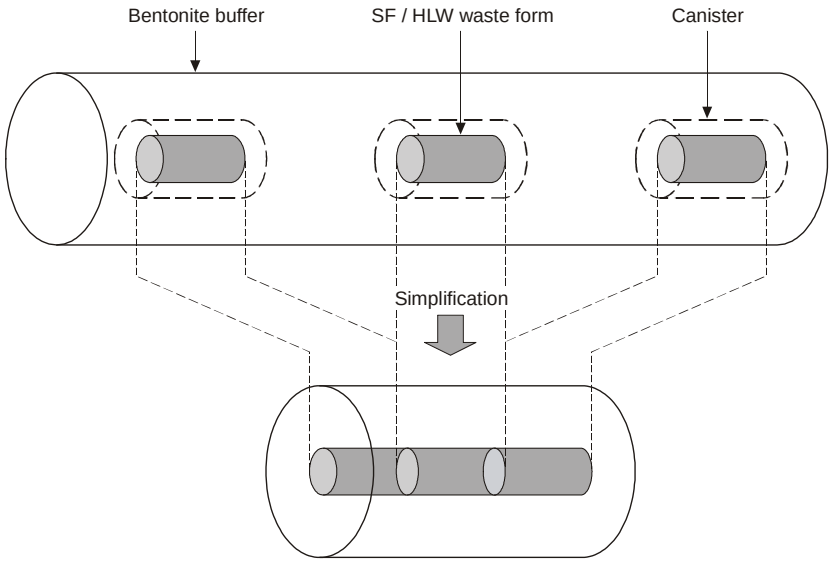

Figure 7: Geometrical simplification for modelling of radionuclide transport through the SF/HLW bentonite buffer (from NAGRA, 2002c).

The physico-chemical data used for this exercise are the same as those of the Reference Case and are summarized in Appendix A. Boundary conditions and geometrical parameters for the FRAC3DVS calculation are summarised in Table 5.

Table 5: Boundary conditions and geometrical parameters for FRAC3DVS.

Boundary	Length [m]	Hydraulic boundary condition	Mass transport boundary condition
AA' and *BB'*	40 m	fixed head	zero concentration
AB and *A'B'*	80 m	no flow	zero gradient normal to boundary
inner boundary of FRAC3DVS domain	1.05 m (diameter)	no flow	mass flow from SPENT calculation

The thickness of the bentonite layer was increased for numerical reasons by 2 cm. With FRAC3DVS it is not possible to implement a hydraulic no-flow boundary and to fix the radionuclide mass transport for this boundary.[9] The domain was therefore extended by 2 cm into the interior. The resulting new inner boundary (boundary E in Figure 8) is a hydraulic and transport no-flow boundary. The solute mass from the near-field calculation is then added in the domain on nodes at the position of the „original" boundary (boundary F in Figure 8).

3.4 CASE 2: Geometry and boundary conditions for a model of glaciation induced flow

The conceptual model and its underlying assumptions are identical to those of the Reference Conceptualisation except in the treatment of radionuclide transport through the bentonite and Opalinus Clay. Advective transport is driven by glacially-induced flow, evaluated over a one million year period. In the course of the next million years, a periodic series of 10 glaciations is assumed to occur (with an assumed frequency of one glaciation every 10^5 years), starting at 50 000 years from today. The duration of each glaciation is taken to be 20 000 years, with an assumed ice shield thickness of 200 m for eight glaciations and 400 m for two glaciations (fourth and tenth event).

As a result of these glaciations, periodic elastic compaction and rebound of the clay barrier (bentonite and Opalinus Clay) occurs, leading to spatial and temporal changes in the groundwater flow in the clay barrier. The clay barrier is assumed to remain homogeneous, i.e. no fracturing occurs before, during or after ice loading. Flow and transport modelling is based on a 2D vertical cross-section through the repository representing a single SF emplacement tunnel and the surrounding Opalinus Clay (Figure 8). The presence of neighbouring emplacement tunnels is taken into account by requiring zero flow and transport over the vertical boundaries (Figure 6). Water flows along the access tunnel system are neglected in the calculations. This is shown to be a valid assumption for a number of different situations (NAGRA, 2002c), and is,

[9] With a first first-type transport boundary condition it is not possible to accurately control the mass-flux into the model domain and a second-type transport boundary condition results in a uncontrollable diffusion of mass out of the model domain. A third-type condition is reduced to a first-type condition if the Darcy flux is set to zero.

therefore, also expected to be a reasonable assumption in the present context of glaciation-induced flow.

Because of the dominant contribution of SF to calculated doses, the analysis is conducted for SF only and is limited to those radionuclides that dominate the summed dose maximum of the Reference Case (organic ^{14}C, ^{36}Cl, ^{41}Ca, ^{79}Se, ^{129}I). The rate of radionuclide release from the SF canisters to the bentonite as a function of time is imposed at boundary F and is taken to be identical to that of the Reference Case.

FRAC3DVS input data for the Base Case related to glacially-induced flow are listed in Appendix A, including radionuclide-dependent data, source term information and data on bentonite and Opalinus Clay.

Table 6: Hydraulic and transport boundary conditions for boundaries A-F (see Figure 8).

Parameter	**Unit**	**Value**	**Data source / Remarks**
hydraulic head at boundary A	m	0	
concentration at boundary A	mol m^{-3}	0	zero concentration boundary
hydraulic head at boundary B	m	80	depends on gradient and model dimensions
concentration at boundary B	mol m^{-3}	0	zero concentration boundary
boundary C			no-flow boundary for both, flow and transport
boundary D			no-flow boundary for both, flow and transport
boundary E			no-flow boundary for both, flow and transport
boundary F	mol s^{-1}		mass flow out of near field/near field release rates provided by Colenco (Results of near-field calculations)

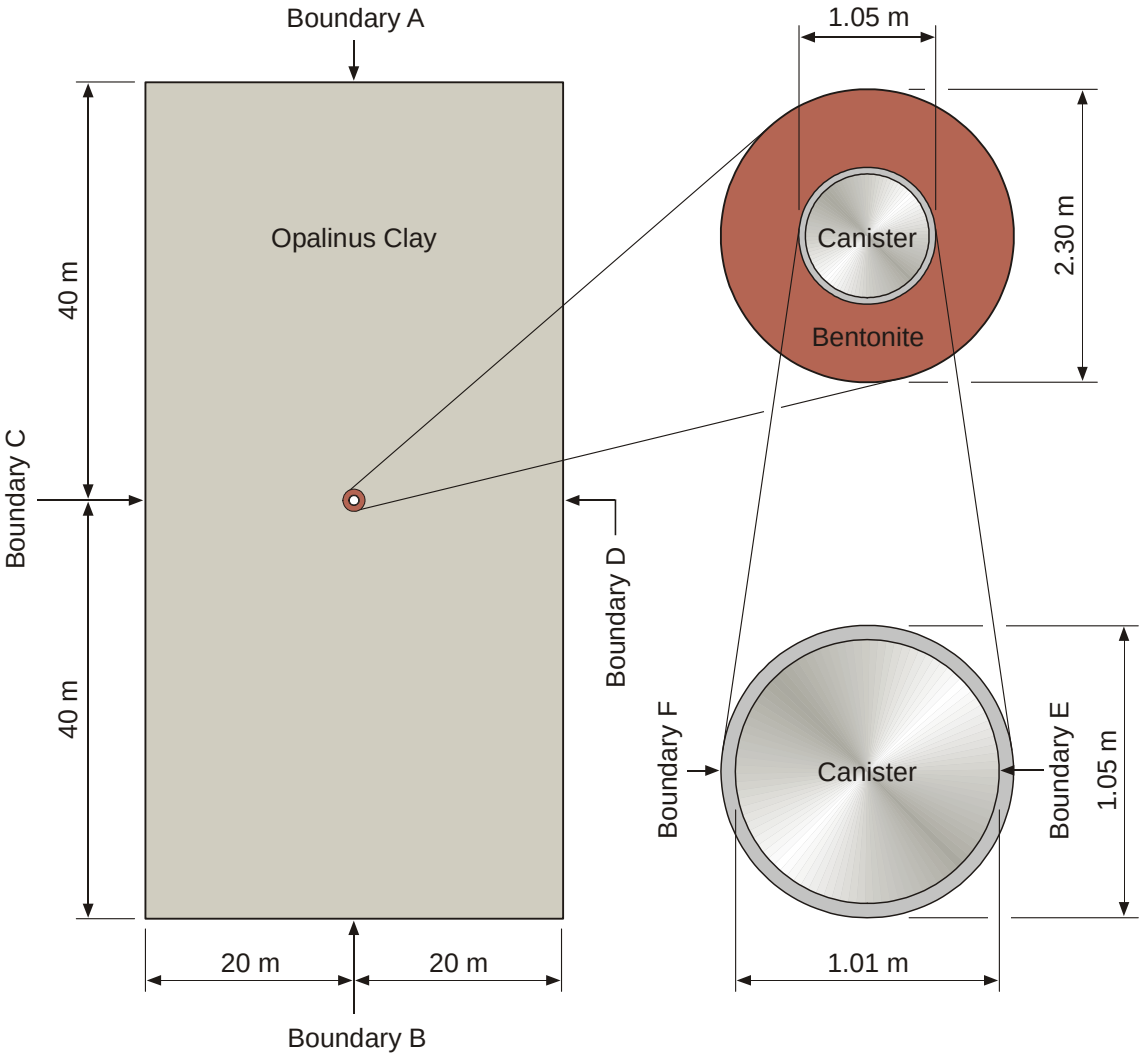

Figure 8: Conceptual model for the calculation of glacially-induced flow and transport in bentonite and Opalinus Clay.

3.4.1 Glaciations - hydraulic heads

The conceptual model for glacially-induced flow in the Opalinus Clay is based on the assumption that the aquifers bounding the host rock provide a direct connection to a discharge area not influenced by glaciation. The discharge area acts therefore as a constant pressure boundary. After the onset of a glaciation, the Opalinus Clay under load finds a new equilibrium via an outflow of water contained in the rock formation. The time needed for equilibration is directly related to the hydraulic conductivity of the medium (see Equation 17). Because the bounding aquifers have a hydraulic conductivity that is 4-6 orders of magnitude higher than that of the Opalinus Clay (see Tab. A3.3-4b in NAGRA, 2002c), the pressure in these aquifers will equilibrate much faster, even if one takes into account the long distance to the discharge area. It is thus conservatively assumed that the bounding aquifers are, compared to the Opalinus Clay, equilibrated instantaneously.[10] This assumption leads to the following idealised situation: At the onset of a glaciation, the hydraulic pressure is instantaneously increased in the Opalinus Clay, but remains as before in the bounding aquifers. For modelling purposes, this situation is equivalent to an instantaneous pressure reduction at the start of a glaciation cycle at the upper (A) and the lower (B) boundary (Figure 8). When the load is removed at the end of a glaciation, the reverse process is applied. Again, the bounding aquifers equilibrate much faster and an instantaneous increase of the reference pressure at the boundaries is implemented in the model.

The assumed sequence of future glaciations and the applied time-dependent hydraulic heads at the boundaries are listed in Table 7. In order to minimise manipulations during simulation runs, the changes of pressure were implemented with a "numerical trick": The flow field was solved with hydraulic heads with respect to a reference level. For the stationary Reference Case the reference level was chosen to be at the upper model boundary (A). In terms of the consolidation process this represents a case where total stress, effective stress and fluid pressure are in equilibrium. During glaciations external (glacial) loading increases the effective stress. In the bounding aquifers this is compensated very fast by a decrease in the fluid pressure, as explained in the previous paragraph. This creates a pressure difference between the Opalinus clay formation and the bounding aquifers. In the numerical model this pressure difference is simulated by decreasing the hydraulic head at the boundaries at the start of a glaciation. to negative hydraulic head values (Table 7). At the end of a glaciation cycle, when the external glacial load is removed, a reverse process is happening. The effective stress is restored to the original value due to unloading. Because the total stress is constant, this needs to be compensated by an increase in the fluid pressure, which happens very quickly in the bounding aquifers. In the numerical model this is simulated by increasing (restoring) the hydraulic heads at the boundaries to their original values at the end of the glaciation.

[10] As the glacial load is transmitted mainly through the solid phase in both formations, the Opalinus Clay formation and the bounding aquifers, the aquifers will not protect the Opalinus Clay formation from an increase in effective stress (see description of the consolidation process at the beginning of Section 2.4)

Table 7: Sequence of future glaciation periods and derived time-dependent hydraulic heads[11] at boundaries A and B from Figure 8 (based on NAGRA 2002a, Section 9.4.8) The times of maximal overburden of 400 m were conservatively chosen in such a way that one of these occurs towards the end of the one million year period considered, where releases from the Opalinus Clay are highest.

Start of period [a]	**End of period [a]**	**Glacial overburden (ice thickness at surface) [m]**	**Hydraulic head at boundary A [m][12]**	**Hydraulic head at boundary B [m] [6]**
0	50000	0	0	80
50000	70000	200	-183.4	-103.4
70000	150000	0	0	80
150000	170000	200	-183.4	-103.4
170000	250000	0	0	80
250000	270000	200	-183.4	-103.4
270000	350000	0	0	80
350000	370000	400	-366.8	-286.8
370000	450000	0	0	80
450000	470000	200	-183.4	-103.4
470000	550000	0	0	80
550000	570000	200	-183.4	-103.4
570000	650000	0	0	80
650000	670000	200	-183.4	-103.4
670000	750000	0	0	80
750000	770000	200	-183.4	-103.4
770000	850000	0	0	80
850000	870000	200	-183.4	-103.4
870000	950000	0	0	80
950000	970000	400	-366.8	-286.8
970000	1000000	0	0	80

[11] The reference datum for the hydraulic heads is the upper model domain, therefore a pressure reduction results in negative hydraulic heads. One could choose another reference datum and convert the negative values into positive ones; that would not change the flow solution.

[12] Calculated assuming a density of ice of 917 kg m^{-3} (see also Appendix A8).

3.5 CASE 3: Geometry and boundary conditions for a model investigating the influence of tunnel convergence

In the Reference Case for SF/HLW, tunnel convergence induced by creep of the Opalinus Clay is considered to be completed before canister breaching, with no effect on radionuclide release. In the Reference Case for ILW, tunnel convergence is assumed to occur during repository construction and resaturation, with little or no deformations of the tunnel cross-section occurring after resaturation of the emplacement tunnels, i.e. after the start of radionuclide release. The current conceptualisation differs from the Reference Case in that alternative assumptions regarding the extent and duration of tunnel convergence are considered, that may lead to enhanced water flow either through the host rock or through the access tunnel system.

In the case of ILW, little convergence is expected after backfilling and (partial) resaturation of the emplacement tunnel due to the strength of the aggregates contained in the cementitious materials (concrete, mortar). There is, however, some uncertainty related to the compaction of void volumes present in the waste containers. In the present conceptualisation, it is assumed that the corroded waste containers (and the structural material) will be partially compacted, leading to tunnel convergence and water displacement (Section 5.4.3 in NAGRA 2002c). Because of the strength of the backfill and the low corrosion rates of much of this material (e.g. stainless steel and Zircaloy) and the relatively low initial porosity, it is expected that the containers will experience limited deformation. Here, it is assumed that the deformation will reduce the porosity by about half. The total reduction in void volume per unit length of ILW-1 tunnel is estimated to be 0.6 $m^3\,m^{-1}$, resulting in a maximal cumulated water displacement for ILW-1 of roughly 100 m^3. Tunnel convergence is assumed to take place within 1 000 years following waste emplacement, in parallel with tunnel saturation. This leads to a convergence-induced water flux of ca. 0.1 $m^3\,a^{-1}$. No calculations are performed for ILW-2, because the total void volume per unit tunnel length and the overall inventory are lower than for ILW-1 (see NAGRA 2002c).

In the framework of a model variant for ILW-1, a pulse of water containing dissolved radionuclides is assumed to be released from the ILW emplacement tunnels through the Opalinus Clay due to tunnel convergence (transient water flows in the Opalinus Clay assumed). In this calculation, radionuclide transport is assumed to take place through the Opalinus Clay only, i.e. the sealings are taken to be impermeable. An upward directed hydraulic gradient of 1 m m^{-1} is imposed in the Opalinus Clay, spanned by the hydraulic heads in the Sandsteinkeuper and the Wedelsandstein. In addition, a source of water, maintained for 1 000 years and with a constant water flow rate of 0.1 $m^3\,a^{-1}$, is assumed in a plane, corresponding to the horizontal cross-sectional area of two ILW-1 emplacement tunnels (9 m × 180 m; from NAGRA, 2002b). Radionuclide transport is assumed to occur by advection and diffusion from the ILW-1 emplacement tunnels both upwards and downwards through the Opalinus Clay, considering transient water flow rates. The analysis is limited to those radionuclides that dominate the summed dose maximum of the Reference Case (organic ^{14}C, ^{129}I).

In the transient model variant considering a pulse of water conveying dissolved radionuclides from the ILW-1 emplacement tunnels through the Opalinus Clay only, the model chain STALLION-FRAC3DVS-TAME is employed. The source term, calculated by STALLION, is identical to the one used in the Base Case. For geosphere transport, FRAC3DVS is employed instead of PICNIC because the transient nature of tunnel

convergence leads to a time-dependent flow field in the Opalinus Clay. The coupled flow and transport Equations 1 and 4 are solved in FRAC3DVS for a 1D porous medium representing the Opalinus Clay (Figure 9 and Table 8).

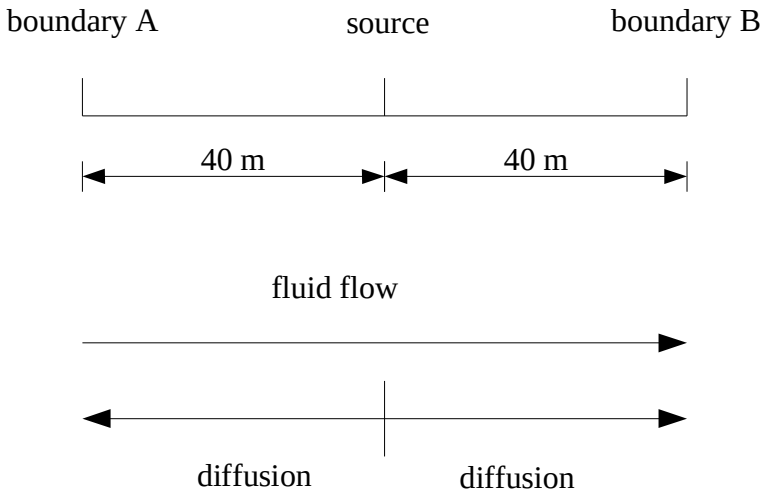

Figure 9: Geometry, boundary conditions and processes considered for the calculations. Boundary A is the lower geosphere boundary and boundary B the upper geosphere boundary.

Table 8: Hydraulic and transport boundary conditions for boundaries A and B (see Figure 9).

Parameter	**Unit**	**Value**	**Data source / Remarks**
hydraulic gradient in OPA	m m^{-1}	1	NAGRA (2002a)
concentrations at geosphere boundaries	mol m^{-3}	0	NAGRA (2002a)
mass flow at near field/geosphere boundary	mol s^{-1}	depends on nuclide and calculation case	Provided by Colenco (Results of near-field calculations)
cumulative fluid volume released by tunnel convergence	m^3	100	NAGRA (2002c)
source fluid flow (boundary condition in FRAC3DVS)	m^3 m^{-2} a^{-1}	$6.17 \cdot 10^{-5}$	see also discussion in NAGRA (2002c)
hydraulic head at boundary A	m	80	
concentration at boundary A	mol m^{-3}	0	zero concentration boundary
hydraulic head at boundary B	m	0	
concentration at boundary B	mol m^{-3}	0	zero concentration boundary

4 Results and discussion

This section presents the results of the three model cases. In subsection 4.1 the results of the one-dimensional PICNIC reference model are compared to the two-dimensional FRAC3DVS model. The second case is presented in subsection 4.2. The effect of glaciations on the radionuclide transport in the two-dimensional FRAC3DVS model is investigated and the results are compared to the FRAC3DVS reference model. In subsection 4.3 the effect of a transient flow field due to tunnel convergence on the transport of radionuclides through the geosphere is shown.

4.1 Comparison between 1D and 2D transport models

The reference model chain calculations using the STMAN-PICNIC are based on several simplifications and result in a one-dimensional model approach. This simplified conceptional model could not be used to calculate transport influenced by consolidation with FRAC3DVS. A two-dimensional reference model for FRAC3DVS was therefore created and the results of the transient flow calculations were compared to this model. As a by-product the results of the FRAC3DVS reference model can be used to investigate the effect of the simplifications applied in the STMAN-PICNIC reference model chain.

4.1.1 Diffusion versus Advection in the reference case

Transport in the reference models is dominated by diffusion. Advection is of minor importance. Figure 10 illustrates the spatial and temporal evolution of normalised concentrations for ^{129}I. The geometry and the setup of the model is described in section 3.3 and the values for the material parameters are summarized in appendix A. The release of radionuclides starts at t = 10 000 years just after canister breaching. In the first hundred thousand years the radial diffusion is the dominating transport mechanism. For later times, the side boundaries hinder the radial diffusion and the upper and lower boundaries dominate the diffusion behaviour. At the source region radial diffusion is dominant, whereas near the upper and lower boundaries the diffusion behaviour is essentially one-dimensional towards the boundaries.

Advection influences the concentration distribution only moderately, there is only a slight asymmetry visible between the upper and lower half of the model domain for later times (lower right picture in Figure 10). *A comparison of the mass flow rates over the model boundaries shows that for ^{129}I the mass flow is 2.2 times higher at the upper boundary compared to the lower boundary.*

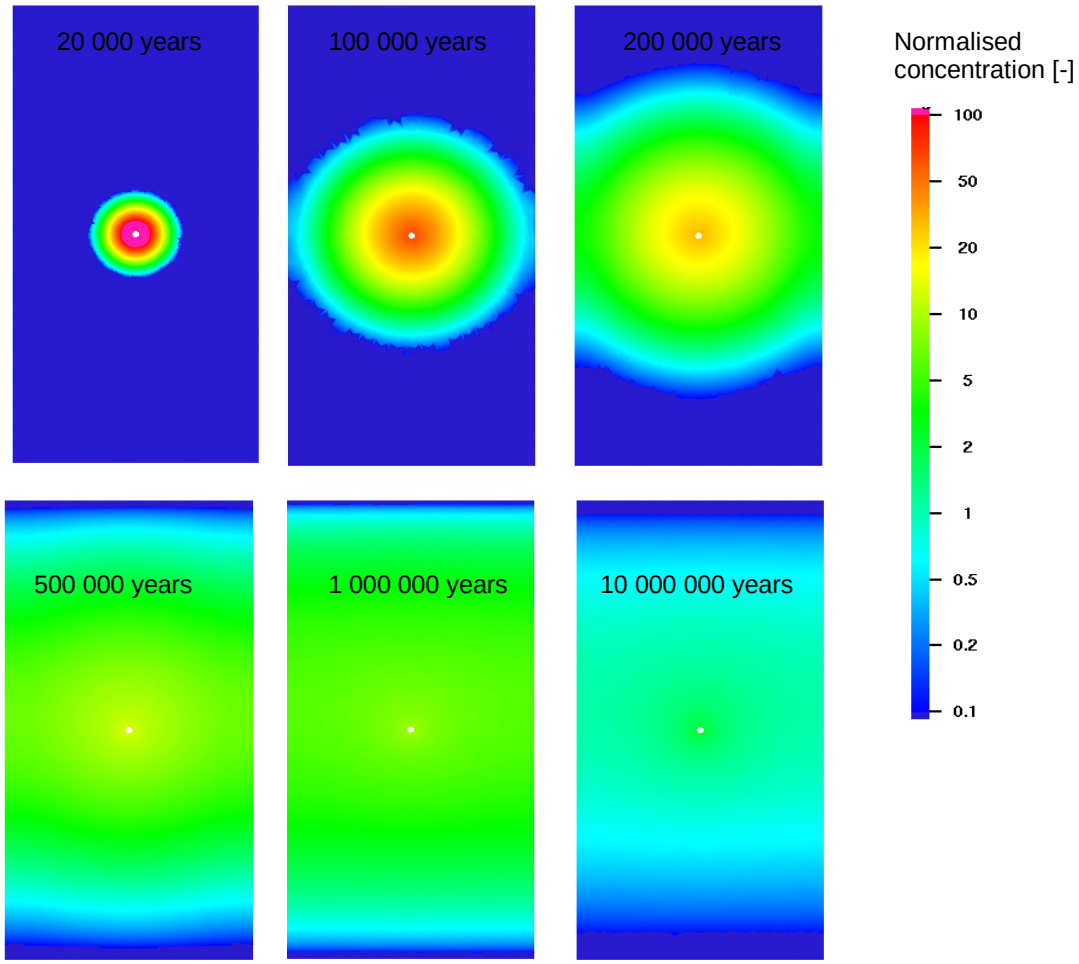

Figure 10: Normalised concentrations in the two-dimensional model domain at different times. At 10 000 years the release of radionuclides starts due to canister breaching. The colours show concentrations on a logarithmic scale over three orders of magnitude.

4.1.2 Effect of model dimensionality on the transport

Figures 11 to 15 summarize the results of the calculations for selected radionuclides. Each figure shows the geosphere release rates of the two-dimensional FRAC3DVS model and the one-dimensional reference model chain. The results of the PICNIC and FRAC3DVS calculations are very similar. In general, FRAC3DVS calculations show slightly lower mass flow rates and the release maxima are reached later compared to those from the PICNIC calculations. These observations are summarized in Table 9, where the times of maximal mass flow rates (peak times) and the peak time values are listed for the different radionuclides.

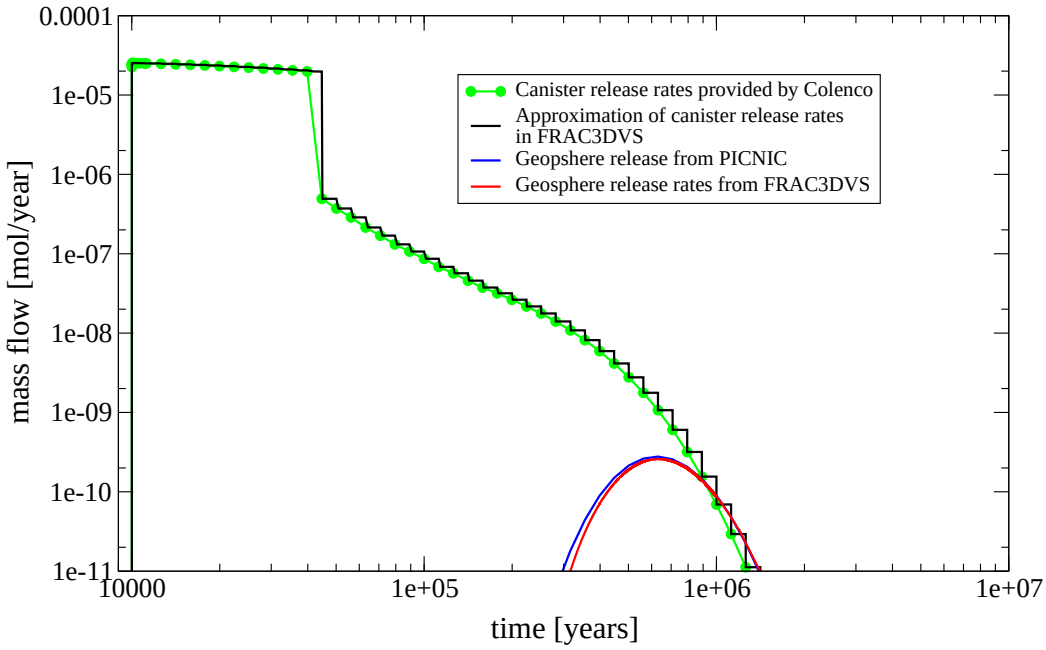

Figure 11: Comparison of the geosphere release rates for ^{41}Ca calculated with FRAC3DVS and PICNIC.

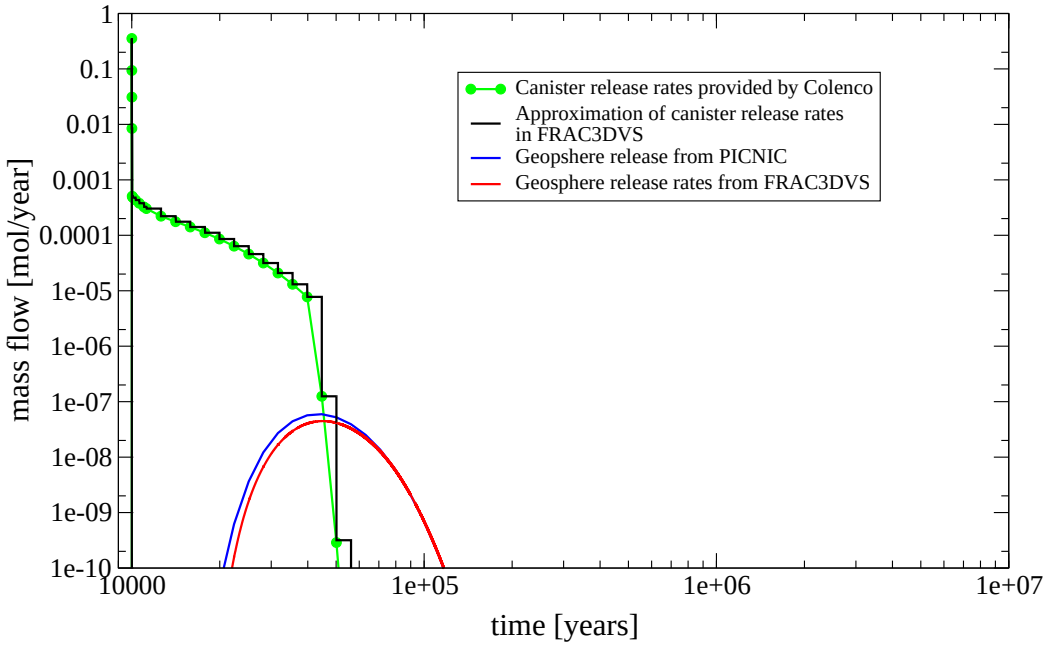

Figure 12: Comparison of the geosphere release rates for organic ^{14}C calculated with FRAC3DVS and PICNIC.

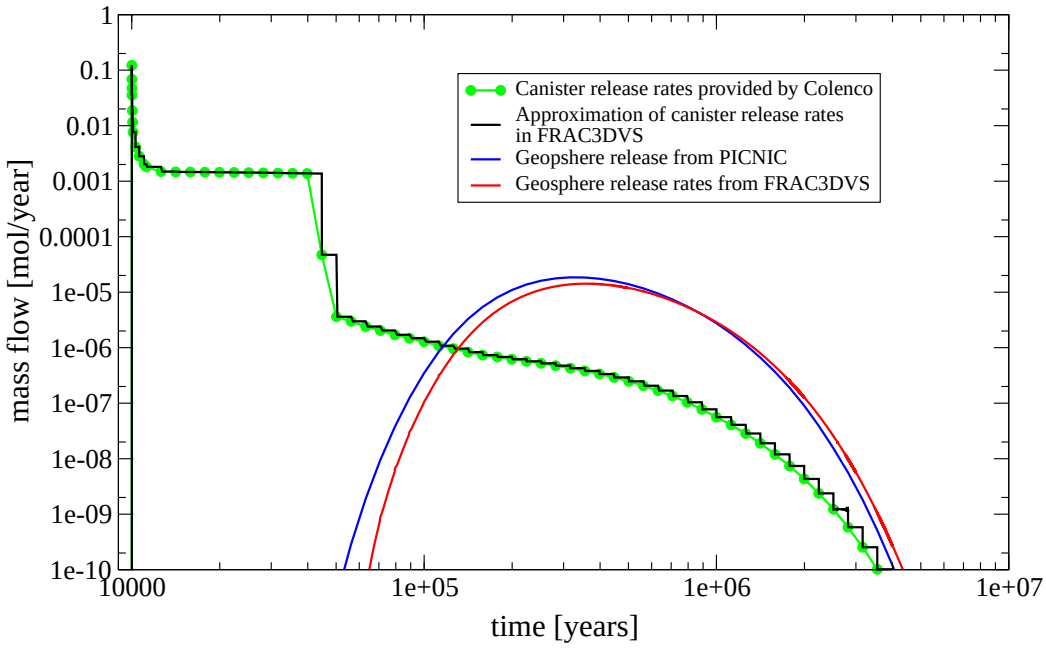

Figure 13: Comparison of the geosphere release rates for ^{36}Cl calculated with FRAC3DVS and PICNIC.

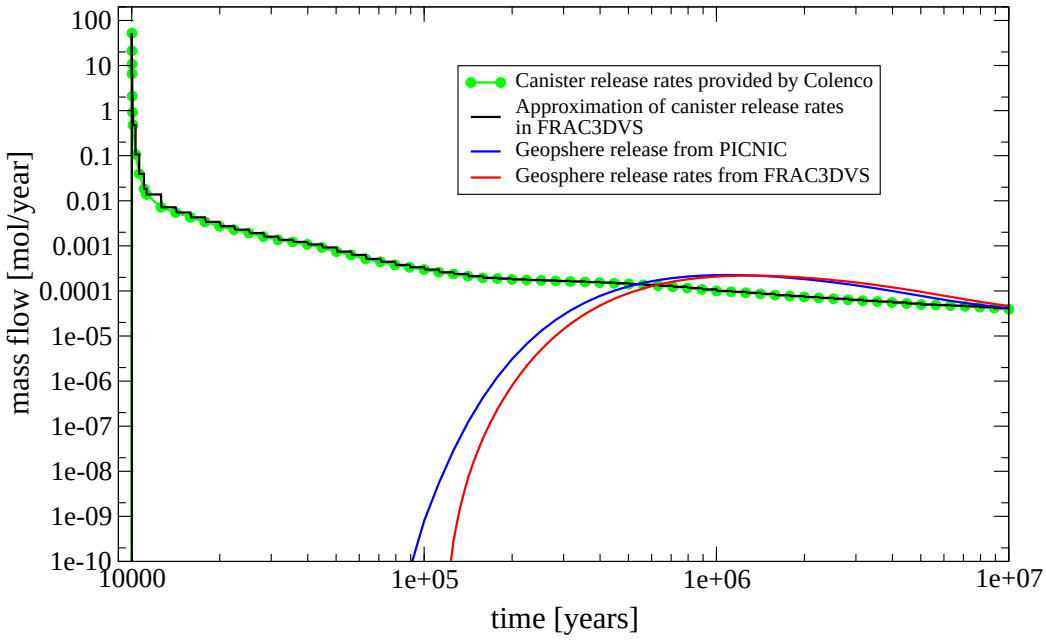

Figure 14: Comparison of the geosphere release rates for ^{129}I calculated with FRAC3DVS and PICNIC.

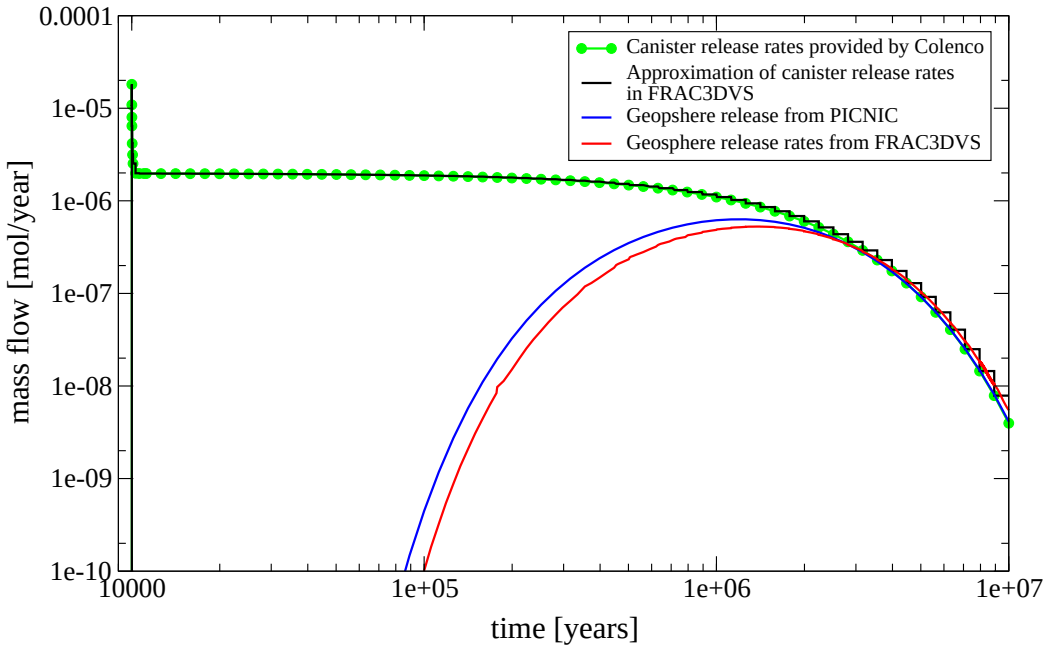

Figure 15: Comparison of the geosphere release rates for ^{79}Se calculated with FRAC3DVS and PICNIC.

The differences visible in Figures 11 to 15 and in Table 9 can be explained by the different dimensionality of the two model approaches. For the one-dimensional model, transport distances are always 40 meters, whereas for the two-dimensional model, the mean transport distances are slightly longer. The minimum transport distance is 39.5 meters (because of the radius of the waste canister) and the maximum distance is about 44.5 meters from the source region to the edges of the model. These slightly higher transport distances cause the shift of the curves towards later times.

Due to the two dimensional geometry of the system radionuclides are also distributed horizontally into the domain. This “dilution” results in a broadening of the release rate curves and in a slight decrease of the maximal release rates.

Table 9: Maximum release rates and times of these maxima for some chosen radionuclides, calculated using PICNIC and FRAC3DVS.

Radionuclide	**PICNIC results**		**FRAC3DVS results**	
	max. release rate [mol a^{-1}]	**time of max. [a]**	**max. release rate [mol a^{-1}]**	**time of max. [a]**
$^{14}C_{org}$	$5.9 \cdot 10^{-8}$	$4.5 \cdot 10^{4}$	$4.5 \cdot 10^{-8}$	$4.5 \cdot 10^{4}$
^{41}Ca	$2.8 \cdot 10^{-10}$	$6.3 \cdot 10^{5}$	$2.6 \cdot 10^{-10}$	$6.3 \cdot 10^{5}$
^{36}Cl	$1.9 \cdot 10^{-5}$	$3.2 \cdot 10^{5}$	$1.4 \cdot 10^{-5}$	$3.6 \cdot 10^{5}$
^{129}I	$2.3 \cdot 10^{-4}$	$1.3 \cdot 10^{6}$	$2.2 \cdot 10^{-4}$	$1.3 \cdot 10^{6}$
^{79}Se	$6.3 \cdot 10^{-7}$	$1.3 \cdot 10^{6}$	$5.3 \cdot 10^{-7}$	$1.4 \cdot 10^{6}$

4.2 Glacially-induced flow in Opalinus Clay

The transport calculations in the previous section 4.1 demonstrated that the advective transport of radionuclides is of minor importance for the reference case. For consolidation driven transport much higher fluid velocities are expected for certain time periods than in the reference case. This should also increase the importance of the advective transport for the overall transport. Advective transport calculations are highly dependent on the accuracy of the flow solution. Calculated Darcy fluxes are therefore first compared to an analytical solution in section 4.2.1. Section 4.2.2 present the results of the transport calculations and interprets them in comparison with reference model results.

4.2.1 Results of the flow calculations

The mean Darcy flux over the boundaries of the two-dimensional model is compared to a one-dimensional analytical solution (TERZAGHI & PECK, 1948). This analytical solution and the calculation of the consolidation-induced flow in FRAC3DVS is summarized in section 2.4.1.

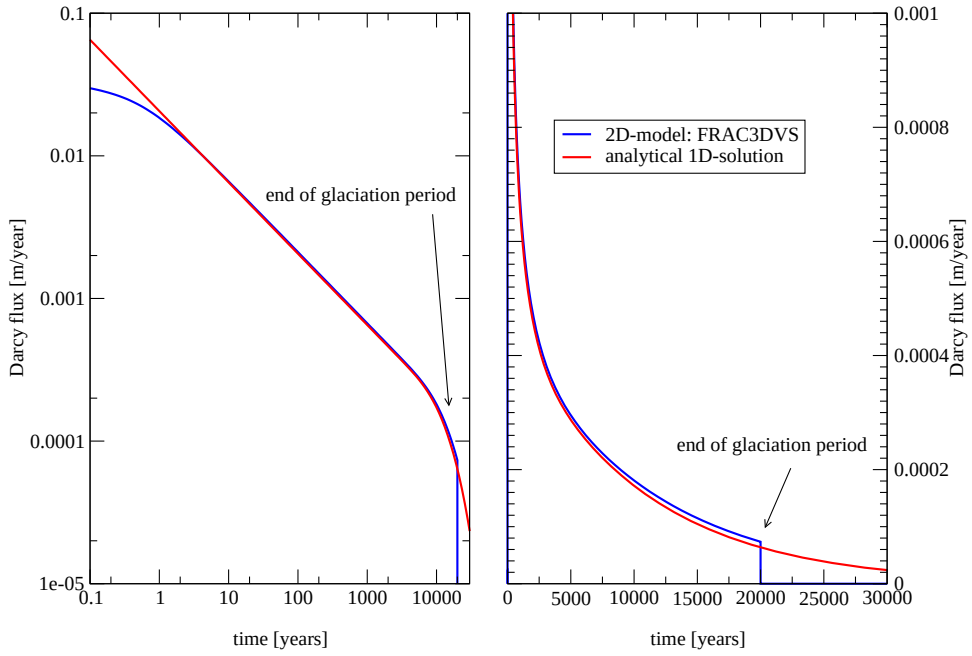

Figure 16: Mean Darcy flux over the geosphere boundaries during a glaciation with 200 meter ice thickness. The blue line shows the fluxes for the 2D-model calculated with FRAC3DVS and the red line is the result of a 1D analytical solution. The glaciation starts at the time t = 0 years.

Figure 16 shows a comparison of the mean Darcy flux (i.e. Darcy flux over the upper and lower model boundaries) of the two-dimensional FRAC3DVS model, with the one-dimensional analytical solution. The mean Darcy fluxes were extracted from the model by summing up the flow rate over all boundary elements and dividing this overall flow rate by the boundary area. The differences between the upper and lower boundary is a

constant upward directed flux of $2 \cdot 10^{-14}$ m/s ($6 \cdot 10^{-7}$ m/a) due to the natural hydraulic gradient between the lower and the upper boundary.

The comparison of the one-dimensional solution and the FRAC3DVS model shows a good approximation of the flow field within FRAC3DVS. Shortly before the end of the glaciation period, the mean Darcy flux out of the model is slightly higher than expected from the analytical solution. This can be attributed to the higher specific storage coefficient for the bentonite filling of the emplacement tunnels. This increases the amount of fluid driven out of the formation and causes slightly higher fluxes compared to the fluxes from the analytical solution (which solves the problem for a homogeneous domain).

For very small times, t<1 year, the numerical deviates from the analytical solution. As can be seen from Equation 17, the analytical solution tends to infinity for z=0 if the time tends to zero. The hydraulic gradient at the boundary gets infinite at the moment of the change. Numerically this behaviour cannot be represented due to the limited spatial and temporal discretization. The numerical approximation therefore does not reproduce the analytical solution for very small times. Nevertheless calculated fluid velocities at the boundaries are also very high in the numerical model. Their absolute values for small times depend on the chosen combination of discretization (near the boundary) and time step length.

4.2.2 Results of the transport calculations

The results of the transport calculations are shown in Figures 17 - 21. The geosphere release rates for the two-dimensional FRAC3DVS model are plotted with and without the influence of glaciations. The overall release curves to the biosphere are nearly identical for all radionuclides in both cases.

A simple calculation of the overall change implied by a single glaciation shows that the effect on the overall transport is expected to be small. The total (additional) water outflow per unit surface area of the Opalinus Clay formation caused by an ice layer of 200 meter is the head change caused by the load (200 m x 917 kg m^{-3} / 1000 kg m^{-3} = 183.4 m) times the specific storage coefficient ($1 \cdot 10^{-5}$ m^{-1}) times half the thickness of the Opalinus Clay formation (40 m). We take only half the thickness, because approximately half of the flow is over the upper and half over the lower formation boundary. For a unit surface of each boundary we have an outflow of 0.073 m^3 of water. If we assume a porosity of 0.1 for the Opalinus Clay formation, the water up to a distance of 0.73 m to the upper or lower formation boundary will be additionally moved out of the formation. Only radionuclides already migrated into these two zones near the boundaries are affected by this additional advective transport mechanism. A doubling of the glacial load, will also double the thickness of the zone and approximately double the amount of radionuclides additionally driven out of the formation. Because of the nonlinear time-dependent behaviour of the water fluxes (Darcy velocities) at the formation boundaries, the release rates might be relatively high at the beginning of the glaciation period, but the overall amount released during the glaciations is limited by the amount already diffused near the boundaries.

There is a linear relationship between the water release, the thickness and the specific storage coefficient of the Opalinus Clay formation, and the thickness of the glacial load. It is clear that a change in one of these parameters changes the overall fluid release with the same factor, and in a first approximation also the overall radionuclide release.

The release rates will vary in a nonlinear way, according to Equation 17. It should be mentioned, that a change in the thickness of the Opalinus Clay formation (e.g. by taking into account the so called “Rahmengesteine” which have similar material properties to the Opalinus Clay) will increase both, the overall amount of water driven out of the formation and the magnitude of the Darcy fluxes. But as diffusion is a very slow process, the radionuclides will reach the regions from which water is driven out of the formation during glaciations much later and e.g. radioactive decay can decrease the amount of radionuclides stored near the formation boundaries.

In the calculations an elastic behaviour of the Opalinus Clay formation is assumed. Elastic behaviour means, that the porosity remains constant during the simulations. As the Opalinus Clay is an overconsolidated sediment, which has already seen pressures much higher than the ones from glacial load, the assumption of elasticity seems appropriate for the pressures (see also Section 5.7 in NAGRA, 2002a). Even if one assumes that the pore space is reduced during each glaciation cycle, this will only slightly affect the transport behaviour. Decreasing the pore space would result in a reduction of the compressibility and in the specific storage coefficient; hence the additional release of radionuclides due to compaction would get smaller. It is relatively easy to perform a simple approximation of the effect if the assumption of elasticity is not met, i.e. that outflow of water is completely compensated by a reduction of porosity. From the definition of the specific storage coefficient it is clear, that per meter hydraulic head increase $1 \cdot 10^{-5}$ m^3 fluids are released and the pore space is decreased by the same volume. After ten glaciations (8 x 200 m and 2 x 400 m ice thickness times ice density) the volume reduction is 0.022 and the porosity would decrease from 0.1 to 0.078. This is a relatively moderate change of the porosity and will not affect the transport behaviour of the radionuclide to any high degree.

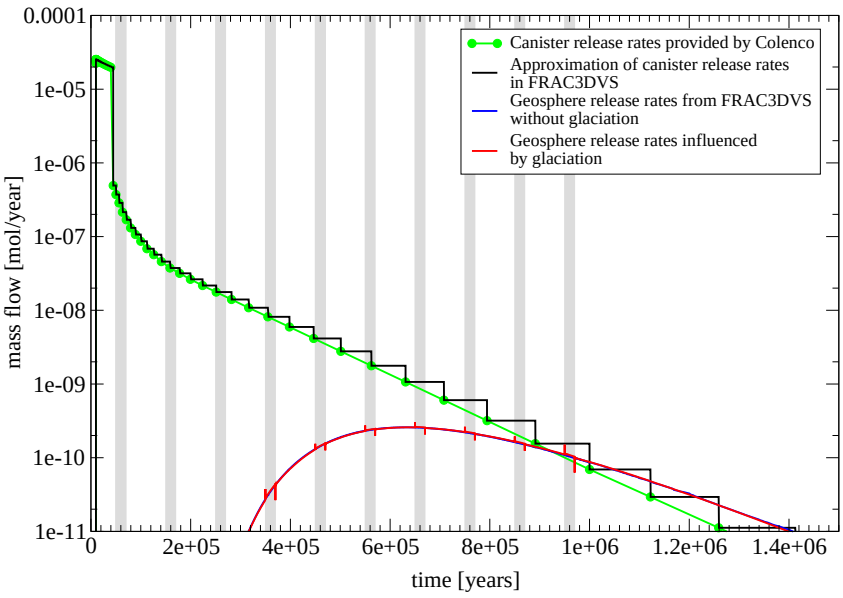

Figure 17: Influence of glaciation induced flow on the geosphere release rates for ^{41}Ca. The release rates for the reference case and for the case influenced by glaciation are nearly identical. A closer view to the curves is given in Figure 22. The shaded areas represent glaciation periods.

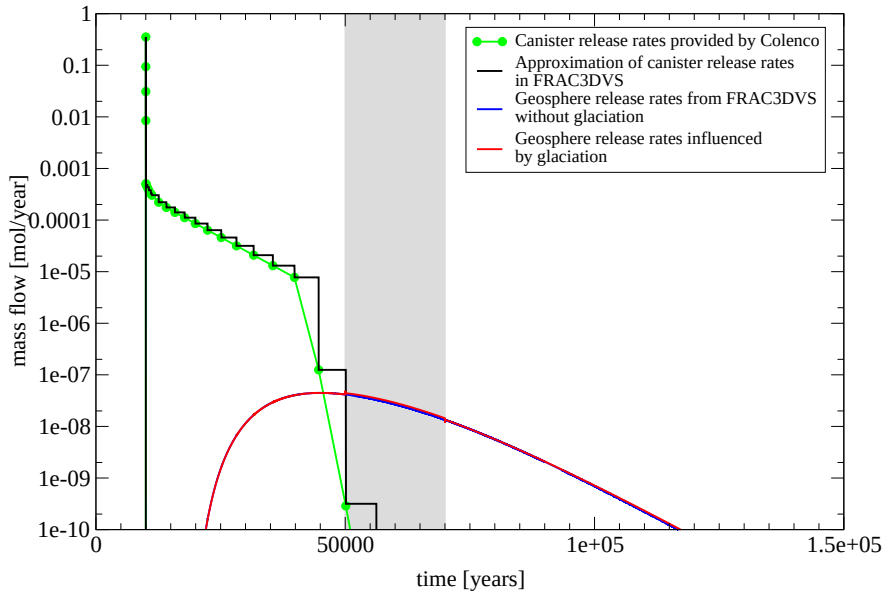

Figure 18: Influence of glaciation induced flow on the geosphere release rates for organic ^{14}C. The release rates for the reference case and for the case influenced by glaciation are nearly identical. A closer view to the curves is given in Figure 24. The shaded areas represent glaciation periods.

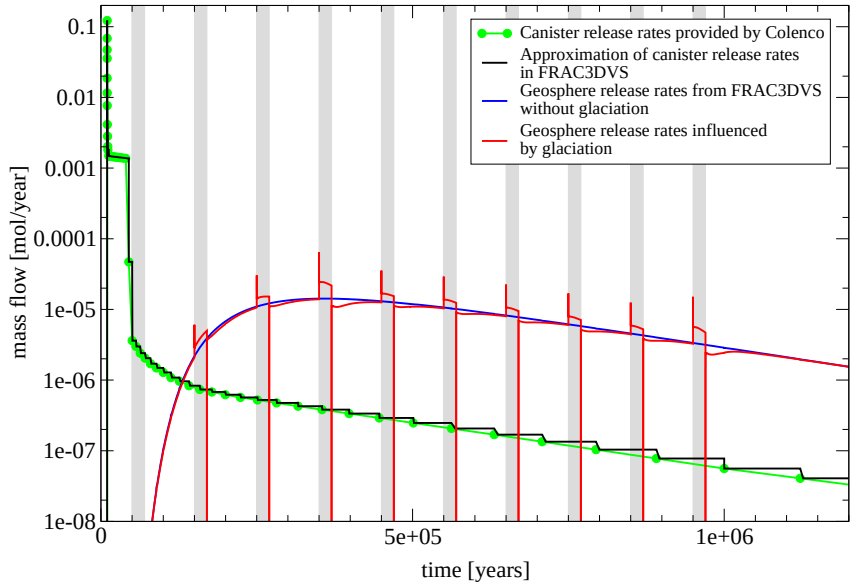

Figure 19: Influence of glaciation induced flow on the geosphere release rates for organic ^{36}Cl. The shaded areas represent glaciation periods.

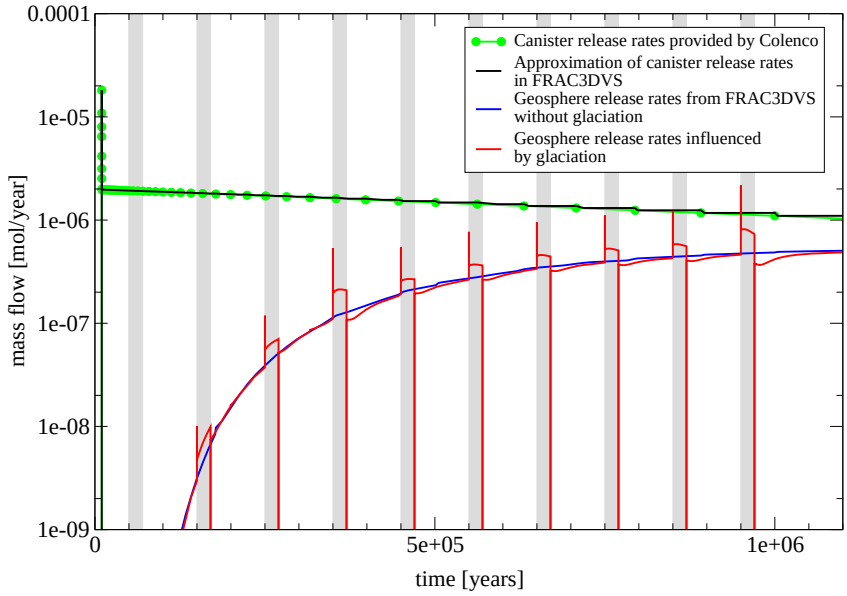

Figure 20: Influence of glaciation induced flow on the geosphere release rates for organic ^{79}Se. The shaded areas represent glaciation periods.

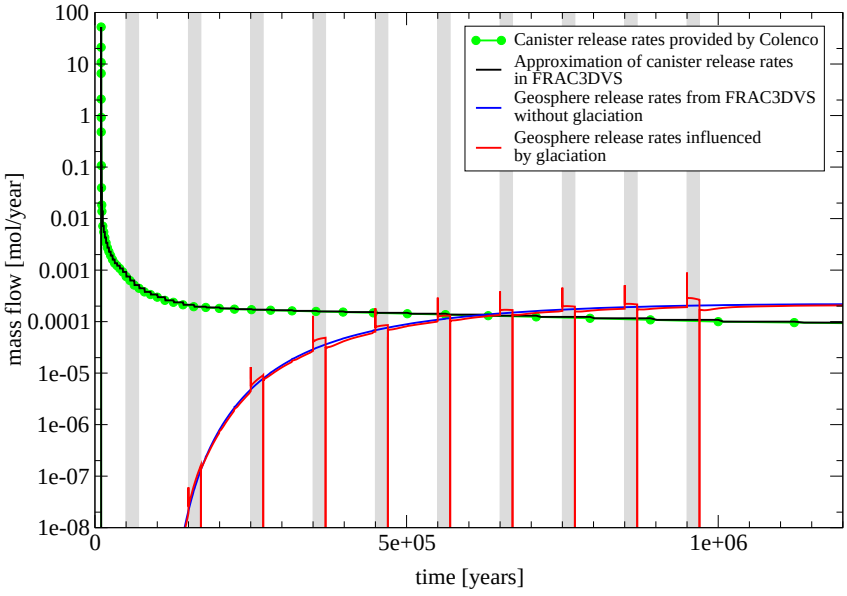

Figure 21: Influence of glaciation induced flow on the geosphere release rates for organic ^{129}I. A closer view to the curves is given in Figure 23. The shaded areas represent glaciation periods.

In Figure 22- Figure 24 details of the breakthrough curves for selected radionuclides (^{41}Ca, ^{14}C and ^{129}I) are additionally shown. During times of glaciation the enhanced advective transport increases the geosphere release rates. After the ice overburden is removed, the hydraulic system recovers (because of the assumed elastic material properties) and fluid flows into the formation. This fluid inflow stops the release of radionuclides for a short time period. The release of radionuclides then increases slowly until release rates similar to the ones of the undisturbed model are reached.

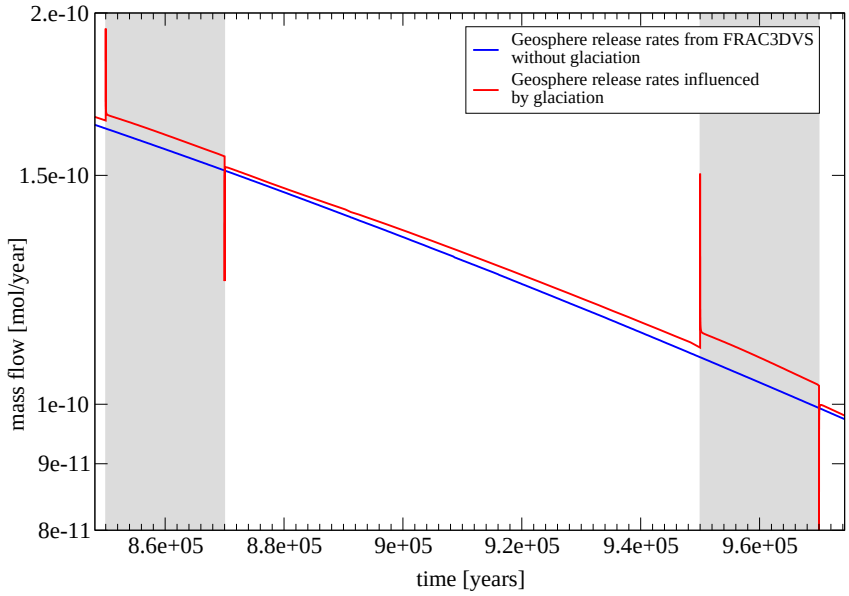

Figure 22: The effect of single glaciation periods on the geosphere release rate for ^{41}Ca. The shaded areas represent glaciation periods.

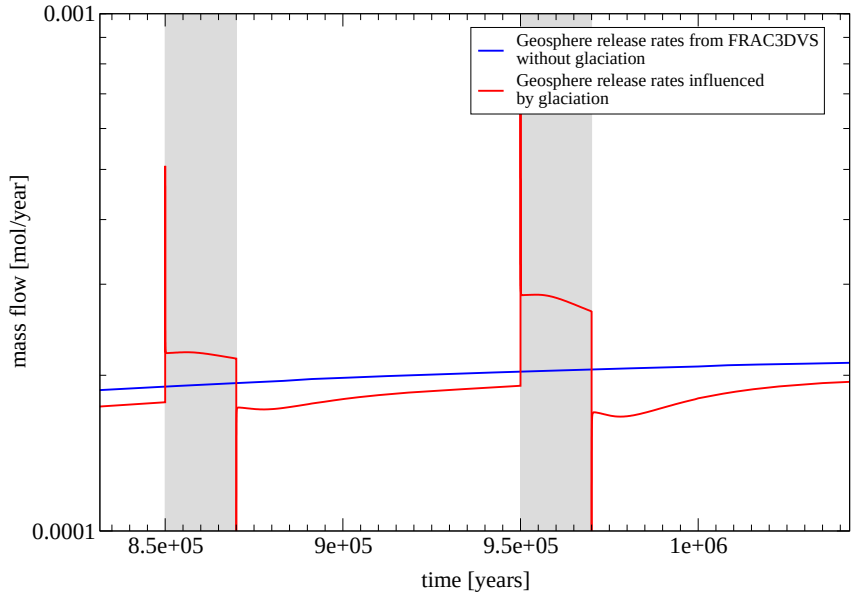

Figure 23: The effect of single glaciation periods on the geosphere release rates for ^{129}I. The shaded areas represent glaciation periods.

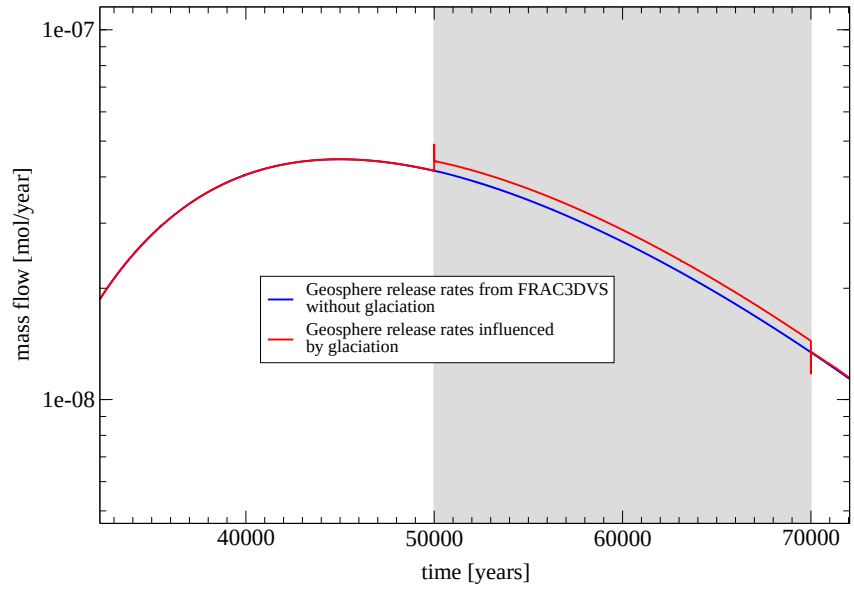

Figure 24: The effect of a single glaciation period on the geosphere release rate for ^{14}C. The shaded area represents the glaciation period.

4.2.3 Influence of the hydraulic boundary conditions on transport

The “spikes”, the increase in the release rates at the beginning of a glaciation, are caused by the singularity in the fluid velocities at the boundaries (see explanation in the previous section). The singularity in the fluid velocities is directly responsible for the singularity in the release rates. Due to numerical reasons it is not possible to calculate the release rates for step changes of the hydraulic heads (beginning and end of glaciation periods) and the height of the “spikes” depends on the smallest utilised time step in the numerical model. The numerical model was set up in such a way, that independent from the time of the glaciation, correct release rates were calculated for more than 1 year after change of the hydraulic boundary conditions. Although the release rates are very high for a short time period after the change of the boundary conditions, the total mass released during this time span is very small. The cumulative amount of ^{129}I released into the biosphere in the first 10 years of the glaciation starting at 0.95 million years is $4.4 \cdot 10^{-3}$ mol. This amount is only about 2 times higher than the amount released in the undisturbed reference case during the same time interval. Table 10 compares the release rates with the reference case release rates for some time intervals. As can be seen, the absolute amount of radionuclides additionally released directly after the change in boundary conditions is relatively small. The increase in the release rate quickly converges to a value higher than the one of the reference case.[13] These spikes would not occur if a realistic continuous growth rate of the glacial burden were used. Unfortunately a change of hydraulic and transport boundary conditions in FRAC3DVS is only implemented as discrete steps, therefore it is in principle not possible to overcome these problems even with a different shape for the hydraulic head change due to glaciation.

Table 10: Comparison of mass release rates during one glaciation cycle (starting at 950 000 years) for the reference case and the case influenced by glaciation for ^{129}I.

Time interval (0 = start of glaciation) [years]	**Integrated release over geosphere boundaries [mol]**	**Mean release rate [mol/year]**	**Mean release rate divided through release rate of the reference model (approx. $2.04 \cdot 10^{-4}$ mol/year)**	**Mean release rate divided by release rate before start of the glaciation (approx. $1.9 \cdot 10^{-4}$ mol/year)**
1	$7.3 \cdot 10^{-4}$	$7.3 \cdot 10^{-4}$	3.6	3.8
10	$4.4 \cdot 10^{-3}$	$4.4 \cdot 10^{-4}$	2.2	2.3
100	$3.2 \cdot 10^{-2}$	$3.2 \cdot 10^{-4}$	1.6	1.7
1000	0.29	$2.9 \cdot 10^{-4}$	1.4	1.5
10000	2.85	$2.85 \cdot 10^{-4}$	1.4	1.5
20000	5.6	$2.8 \cdot 10^{-4}$	1.4	1.5

[13] If the glaciation were to last longer the release rate would decrease slowly against the reference case release rate. The collapse of the flow field after some time (compare the analytical solution in Figure 16) will accelerate this process.

A similar effect can be seen at the end of the glaciations due to reversed flow directions. The main difference is that the lower limit of geosphere release rates is zero, because concentrations at the boundary are assumed to be zero.

4.2.4 Increase of release rates during glaciations

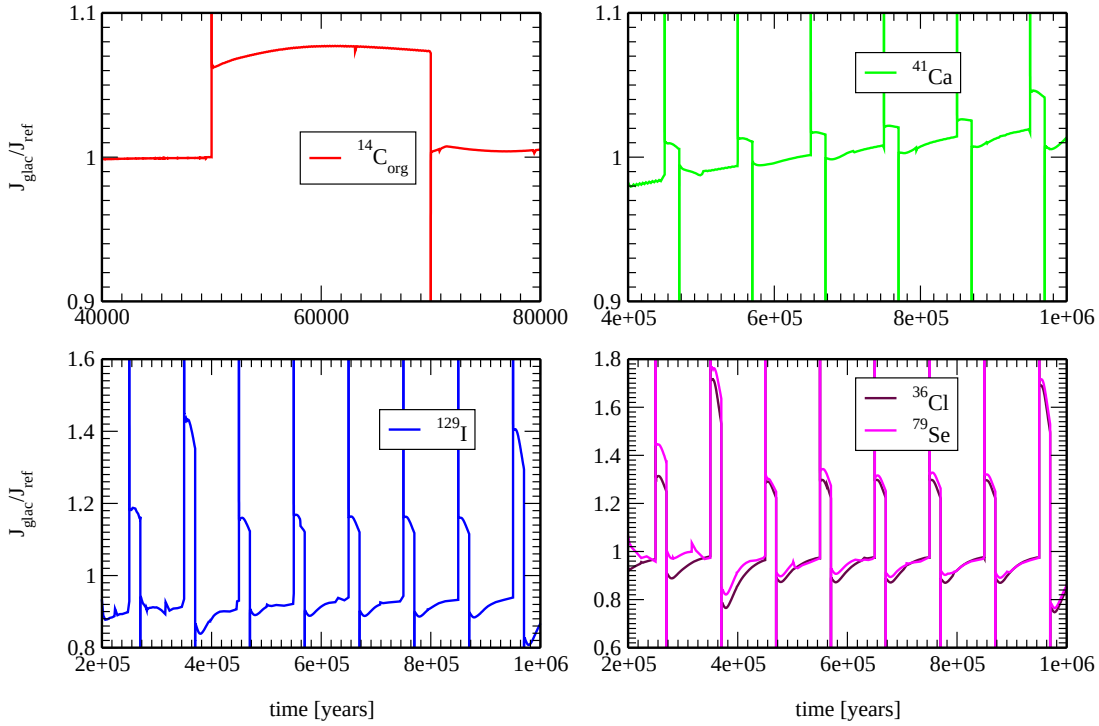

Figure 25: Normalized mass fluxes over the geosphere boundaries for different radionuclides. The geosphere release rates for a model influenced by glaciation J_{glac} were normalized with respect to the 2D reference case release rates J_{ref}.

Figure 25 shows normalized release rates for different radionuclides. The release rates were normalized with respect to the values of the reference case. Not all glaciation periods are evaluated for all radionuclides, because if the release rates are far below 10^{-10} mol/year differences in the release rates are mainly caused by the inaccuracies of the numerical method.

The absolute value of the release rates is important for the accuracy of the calculations. Absolute release rates of less than $1 \cdot 10^{-11}$ mol/year are strongly influenced by numerical errors, such as oscillations, or “spikes” due to changes in the time step length.

The spatial distribution of the radionuclides influences the additional release of radionuclides during the glaciations. There will be no increase in the release rate if there are no radionuclides near the Opalinus Clay boundaries. A heterogeneous distribution of the radionuclides near the boundary can change the form and the height of the release curve.

Until the first glaciation the absolute release rates with and without glaciations are identical and the normalized release rate is constant and has a value of 1. For later glaciations the release rate is lower and the system slowly reaches an undisturbed state again. Relaxation times are in the order of the length of the interglacials (80000 years), which is much longer than the duration of the glaciations (20000 years).

The overall increase in the normalized release rates for ^{41}Ca is due to an underlying inaccuracy in the numerical procedure. If concentrations are decreasing strongly due to radioactive decay the numerical accuracy of the iterative solver is limited and mass flow rates (calculated from the concentrations) converge towards unrealistic high values. Decreasing the time step length reduces the problem, but increases the number of time steps and the calculation times to very high values.

Table 11: Approximate increase of the release rates during glaciations compared to the values of the reference case (without glaciations).

	$^{14}C_{org}$	^{41}Ca	^{129}I	^{36}Cl	^{79}Se
200 m ice thickness	1.08	1.02	1.25	1.35	1.35
400 m ice thickness	-	1.04	1.5	1.7	1.7

The approximate ratios of the release rates in the middle of the two different types of glaciations (approximately 10000 years after the start of the glaciation) are extracted from Figure 25. The values are compiled in Table 11. A first obvious effect is that doubling the ice thickness also doubles the relative increase in the release rates.

As can be seen, the increase of the release rates for cations and neutral species ($^{14}C_{org}$, ^{41}Ca) during glaciation periods is much smaller than for anions (^{79}Se, ^{36}Cl, ^{129}I). For all species (anions, cations and neutral species) geosphere transport is dominated by diffusion and advective transport contributes only during times of glaciation. The Peclet number *Pe* [-] is a measure of the relative importance of advection compared to diffusion:

$$Pe = \frac{\left(v_D / \varepsilon_D \right) \cdot l}{D},$$

where v_D is the fluid velocity, D the pore diffusion coefficient and l a typical length scale. For $Pe \leq 1$ diffusive transport and for $Pe >> 1$ advective transport is dominant. The Peclet number changes for the simulations, because the flow velocities change in space and time due to glaciations. When the typical length scale is connected to the size of the (mesh) element, the so-called “grid Peclet number” gives a measure for the numerical stability of the system and should be smaller than 2 for the applied Galerkin-finite-element approach with semi-implicit (Crank-Nicholson) time-weighting. For higher Peclet numbers oscillations and numerical dispersion influence the solution. Due to the spatial and temporal variability of the fluid velocity it is also possible to interpret the grid Peclet number in a physical sense as a measure of the local relation between diffusive

and advective transport. Table 12 shows a comparison of the grid Peclet numbers at the boundary of the model domain for the reference case without glaciation and for the case with 200 m ice thickness.

Table 12: Grid Peclet number at the boundary of the Opalinus Clay for the reference case without glaciation and for the case with glaciation (ice thickness: 200 meter) at the time of 1000 years after the beginning of the glaciation. As a typical length scale the size of a boundary element of the finite-element mesh was chosen (l=0.5 m).

	Grid Peclet number for reference case without glaciation	**Grid Peclet number 1000 years after start of a glaciation**
non-anions ($^{14}C_{org}$, ^{41}Ca)	$1 \cdot 10^{-3}$	1
anions (^{79}Se, ^{36}Cl, ^{129}I)	$1 \cdot 10^{-2}$	10

Without glaciation the transport is clearly dominated by diffusion, for cations and neutral species, and even more than for the anions. Advective transport is coupled to the fluid velocity, which is calculated from the Darcy flux by division with the flow porosity. As explained in KOSAKOWSKI (2001) the value of the flow porosity is set to the value of the accessible porosity for the specific nuclide. According to Nagra (2002a) anions see a lower porosity (0.06 for Opalinus Clay) as cations and neutral species (0.12 in Opalinus Clay). Lower porosity values lead to higher fluid velocities and to an increase of the effects of advection. Generally this is more pronounced for anions than for cations and neutral species. This is also reflected in the higher release rates during glaciations (Table 11).

For short times after the change of the boundary conditions the grid Peclet numbers are very high next to the boundaries. This introduces numerical dispersion and oscillations into the transport solution. Fortunately flow velocities (and grid Peclet) numbers drop very quickly, oscillations are damped effectively and the transport solution convergences towards the “true” solution.

For the calculated cases where advection dominates the transport for a relatively long time interval during glaciations, the difference in the release rates scales for non-sorbing species with the Peclet number. e.g. the Peclet number for ^{129}I is about 10 times bigger than for ^{41}Ca. This corresponds to the increase in the relative release rates, which is 20% for ^{129}I and 2% for ^{41}Ca.

Another process affecting the increase of the release rates during glaciations is the retardation due to sorption. Non-sorbing radionuclides show higher release rates during glaciations (compare e.g. $^{14}C_{org}$ with ^{41}Ca, or ^{36}Cl and ^{79}Se with ^{129}I). This effect is caused by the delayed migration of radionuclides, compared to the movement of the water, coupled with the decrease of the flow velocities at the geosphere boundary. Compared to non-sorbing radionuclides sorbing radionuclides need a longer timespan to migrate to the boundary. The fluid velocities at the boundary generally decrease during glaciations (see Figure 16) and therefore release rates for sorbing radionuclides are lower.

4.3 Convergence-induced flow in the Opalinus clay

The influence of tunnel convergence on the geosphere release rates is exemplified for the transport of ^{129}I and $^{14}C_{org}$. These two radionuclides represent two extreme cases. ^{129}I is released in relatively high quantities and is retarded only slightly. Maximal rates are reached about 1 million years after the first release into the geosphere. $^{14}C_{org}$ is transported without retardation, but is released only in minor quantities. Other radionuclides are either transported much more slowly in the geosphere (due to sorption processes in the Opalinus Clay), or their release rates are comparable to the two mentioned radionuclides.

4.3.1 Mass balance for fluid flow

As noted previously, the accuracy of the solution of the flow problem is of crucial importance for calculating advective transport processes. In this section we concentrate therefore on the analysis of the spatial and temporal evolution of the flow field.

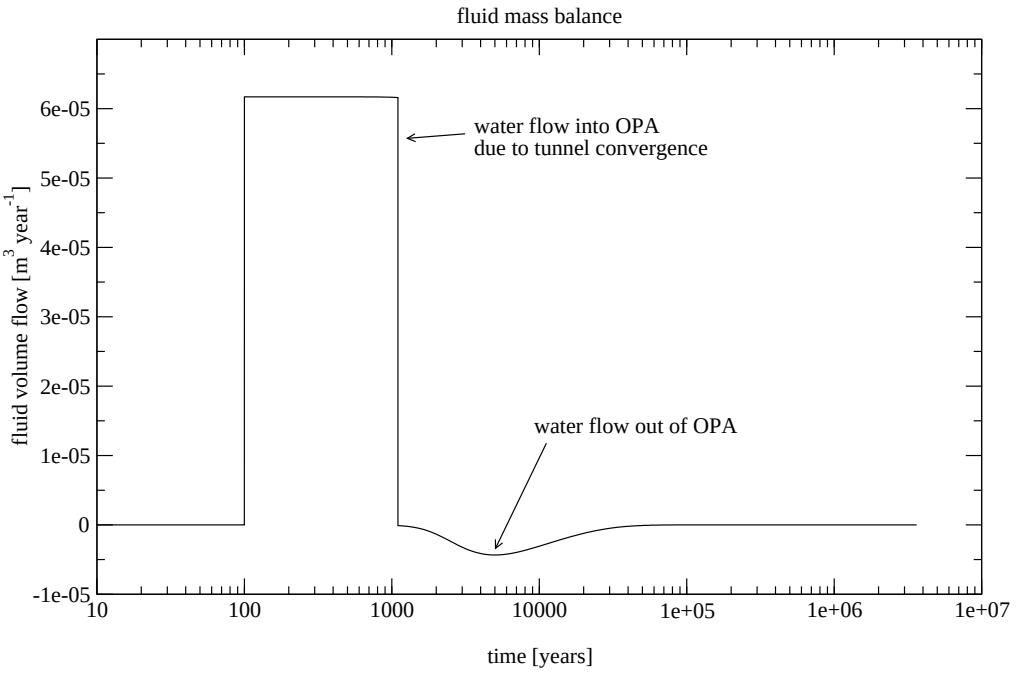

Figure 26: Net water flow through the geosphere. For positive flow rates fluid is stored in the model domain, whereas negative values indicate a release of water. Equilibrium is reached if inflow equals outflow and the overall flow rate is zero.

The mass balance for the model is shown in Figure 26. The time scale is logarithmic. Between 100 and 1100 years water is released to the geosphere with a constant rate due to tunnel convergence. The flow out of the geosphere is delayed due to the low permeability of the Opalinus Clay Formation and the specific storage coefficient of $1 \cdot 10^{-5}\ m^{-1}$.

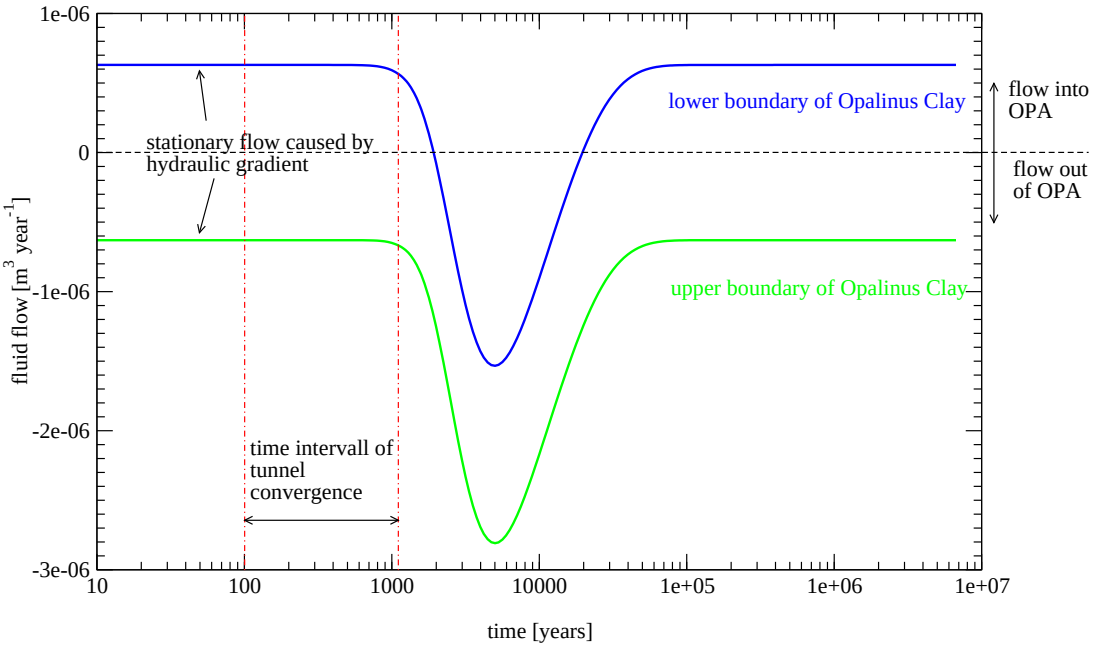

Figure 27: Water flow over the lower and upper geosphere boundary in a logarithmic-linear representation. Normally the lower boundary is an inflow and the upper boundary an outflow boundary. Due to the additional inflow caused by the tunnel convergence the lower boundary is temporarily changed to an outflow boundary, too.

The shape of curve for the water flow during tunnel convergence has the form of a plateau for about 1000 years. The response of the Opalinus Clay formation on the tunnel convergence, visible in Figure 27 in form of the (out)flow maxima at the boundaries, is delayed and dispersed due to the low hydraulic conductivity and the relatively high specific storage coefficient of the Opalinus Clay formation. Maximal fluid velocities at the boundaries are reached after 5000 years.

A fluid mass balance for the numerical model was calculated by integrating the fluid flows over time. There is only a small difference of about 3% between the fluid volumes flowing in and out.

4.3.2 Transport calculations

Figures 28 to 30 show the mass flow rates at the tunnel surface (source boundary condition) and over the boundaries of the Opalinus Clay Formation.

Mass flow rates at the peak maximum for ^{129}I ($^{14}C_{org}$) are 4% (13 %) higher as for the reference case. This increase is mainly caused by the nearly 30% higher radionuclide source term during tunnel convergence. The effect of the additional transient flow field on the radionuclide transport in form of an earlier breakthrough is also very small. Maximum geosphere release rates are reached for ^{129}I ($^{14}C_{org}$) after 1.099 million years (33060 years) in the reference case and after 1.095 million years (32630 years) in the case of tunnel convergence.

In order to make the FRAC3DVS calculations comparable to the reference case calculations applying PICNIC, the two-dimensional transport problem is transferred into a one-dimensional one, assuming that the fluid and radionuclide transport takes place only in vertical directions. The flow rate due to tunnel convergence is then $6.17 \cdot 10^{-5}$ m^3 m^{-2} a^{-1}. This flow rate gives an overall volume of 100 m^3 if released for 1000 years over a rectangular area of 9 meter width (tunnel diameter for ILW-1) and 180 meter length (tunnel length for ILW-1).

With this simplification radionuclides would travel a maximum of 14 cm from the source (either upwards or downwards) if we only consider advection driven by tunnel convergence in the EDZ (porosity 0.22). If one would disregard the EDZ and consider only advection in undisturbed host rock with a porosity of 0.06, this maximal advection distance would increase up to 52 cm (either upward or downward).

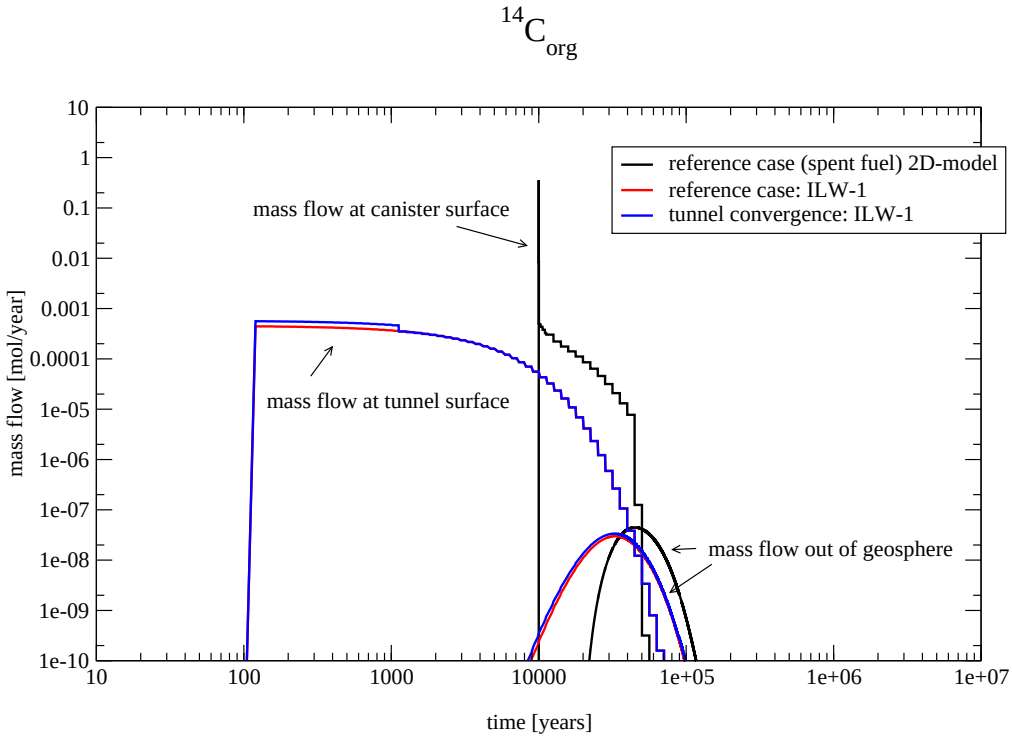

Figure 28: Mass flow rates for ^{14}C into and out of the geosphere for the ILW-1 reference case and the case with tunnel convergence. For sake of comparison the mass flow rates for the spent fuel reference case are also included.

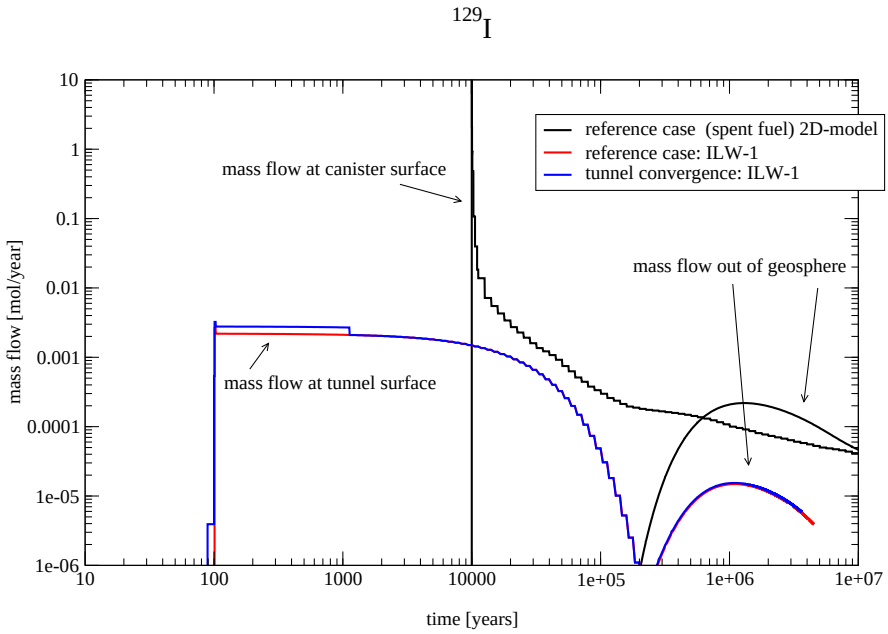

Figure 29: Mass flow rates for ^{129}I into and out of the geosphere for the ILW-1 reference case and the case with tunnel convergence. For the sake of comparison the mass flow rates for the spent fuel reference case are also included.

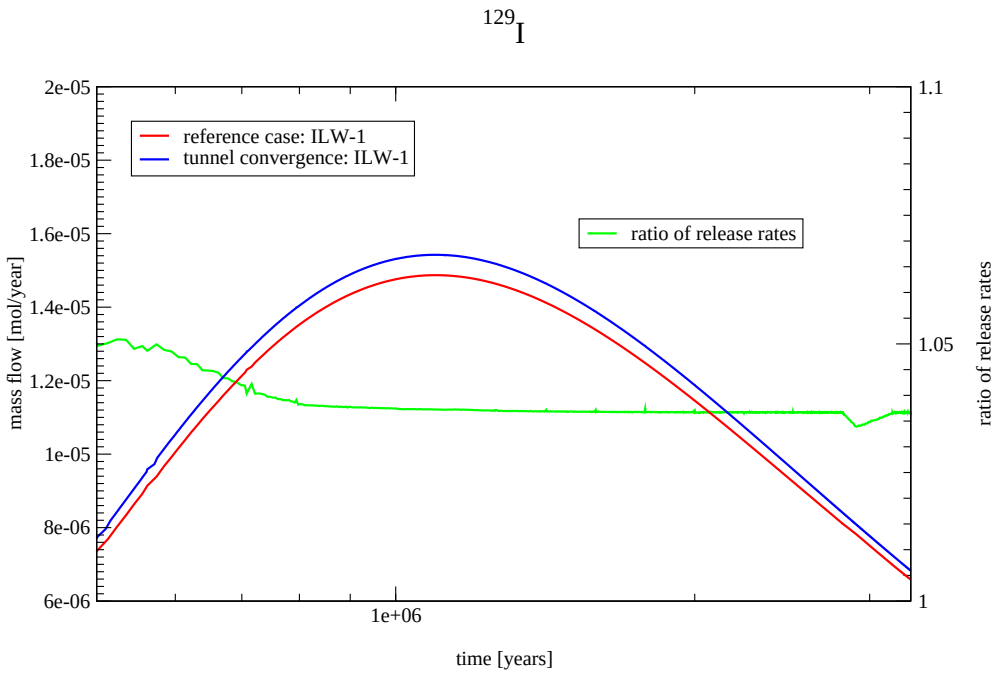

Figure 30: Detail of Figure 29 for the transport of ^{129}I. Additionally the ratio of the mass flow rates out of the geosphere with and without tunnel convergence is drawn (right axis). For the release maximum, the mass flow rate for the tunnel convergence case is only 3.6 % higher than for the reference case.

5 Summary

5.1 Reference case transport and 1D vs. 2D models

The one-dimensional approximation gives results similar to the geometrically more realistic FRAC3DVS model. FRAC3DVS release maxima are, however, slightly lower and occur at slightly later times. This modelling exercise thus gives strong support for the applicability of the one-dimensional approximation. Discrepancies introduced by the one-dimensional approximation are shown to be small and the results are always conservative compared with the more realistic FRAC3DVS calculations.

5.2 Influence of glaciation induced flow

Glaciation induced flow may promote the transport of radionuclides in the geosphere. The release rates for non-sorbing anions during the glaciations are up to 1.7 times higher (compared to the reference case not influenced by glaciation). However, for a time period of about 1 year after the beginning of the glaciations the calculated release rates should be disregarded. These release rates are influenced by an oversimplification in the conceptual model where glaciations start and end instantaneously.

The influence on the transport of cations or neutral species is less than for anions, since the relative importance of the advective transport for anions is higher than for cations and neutral species.

The increase in the release rates during glaciations is lower for sorbing than for non-sorbing radionuclides. This effect is caused by the delayed migration of radionuclides, compared to the movement of the water, coupled with the reduction of the flow velocities at the geosphere boundary.

5.3 Influence of tunnel convergence

The influence of the tunnel convergence on the transport of radionuclides in the geosphere is very small. The geosphere release rates are slightly higher if tunnel convergence is considered. This can be attributed to the higher source term during tunnel convergence. However, the influence of the enhanced advection due to the tunnel convergence on the transport times is very small.

6 Acknowledgements

I would like to thank Andreas Jakob, Ralph Mettier and Paul Smith for their critical reading of different versions of the manuscript. Special thanks go to Jürg Schneider for his numerous helpful comments and suggestions.

The thorough and careful external review by Peter Robinson (Quintessa) highly improved this report.

This work was partially financed by the National Cooperative for the Disposal of Radioactive Waste (Nagra).

7 References

BEAR, J., 1972. Dynamics of fluids in porous media. Dover Publications, New York.

DE MARSILY, G., 1986. Quantitative hydrology. Academic Press, San Diego.

HORSEMAN, S.T., ALEXANDER, J., HOLMES, D.C., 1991. Implications of long-term transient flow , coupled flow and borehole effects on hydrological testing in the Opalinus Clay: Preliminary study with scoping calculations, Nagra Technical Report NTB 91-16, Nagra, Wettingen, Switzerland.

KOSAKOWSKI, G., 2000. Numerical modelling of transient flow due to consolidation. PSI Internal report AN-44-00-17, Paul Scherrer Institut, Villigen, Switzerland.

KOSAKOWSKI, G., 2001. Transport modelling with FRAC3DVS under consideration of different flow and transport porosities. PSI Internal report AN-44-01-08, Paul Scherrer Institut, Villigen, Switzerland.

LANGGUTH, H.-R., VOIGT, R., 1980. Hydrogeologische Methoden. Springer Verlag, Berlin.

NAGRA, 2002a. Projekt Opalinuston - Synthese der geowissenschaftlichen Untersuchungsergebnisse. Entsorgungsnachweis für abgebrannte Brenn-elemente, verglaste hochaktive sowie langlebige mittelaktive Abfälle. Nagra Technical Report NTB 02-03, Nagra, Wettingen, Switzerland.

NAGRA, 2002b. Projekt Opalinuston – Konzept für die Anlage und den Betrieb eines geologischen Tiefenlagers. Entsorgungsnachweis für abgebrannte Brenn-elemente, verglaste hochaktive sowie langlebige mittelaktive Abfälle. Nagra Technical Report NTB 02-02, Nagra, Wettingen, Switzerland.

NAGRA, 2002c. Project Opalinus Clay: Models, Codes and Data for Safety Assessment. Demonstration of disposal feasibility for spent fuel, vitrified high-level waste and long-lived intermediate level waste (Entsorgungsnachweis). Nagra Technical Report NTB 02-06, Nagra, Wettingen, Switzerland.

NAGRA, 2002d. Project Opalinus Clay: Safety report. Demonstration of disposal feasibility for spent fuel, vitrified high-level waste and long-lived intermediate-level waste (Entsorgungsnachweis). Nagra Technical Report NTB 02-05, Nagra, Wettingen, Switzerland.

PATERSON, W.S.B. 1994. The Physics of Glaciers, Third Edition, Pergamon/ Elsevier, Oxford, England.

PFINGSTEN, W., 2000. FRAC3DVS, RANCHMD, PICNIC and MOCTAC code comparison for advective-dispersive-diffusive systems – verification tests and applications. PSI Internal report AN-44-00-14, Paul Scherrer Institut, Villigen, Switzerland.

SCHNEIDER, W., GÖTTNER, J.-J., 1991. Schadstofftransport in mineralischen Tonabdichtungen und natürlichen Tonschichten. Geologisches Jahrbuch Reihe C, 58, 3-132.

TERZAGHI K., PECK, R.B., 1948. Soil Mechanics in Engineering Practice. John Wiley & Sons, New York, USA.

THERRIEN, R., SUDICKY, E. A., 1996. Three-dimensional analysis of variably-saturated flow and transport in porous media. Journal of Contaminant Hydrology, 23, 1-44.

THERRIEN, R., SUDICKY, E.A., MCLAREN, R. G., 1999. User's Guide for NP 3.49 – A preprocessor for FRAC3DVS 3.49: An efficient simulator for three-dimensional, saturated-unsaturated groundwater flow and chain-decay solute transport in porous or discretely-fractured porous formations. University of Waterloo, Manual.

WEAST, R. C., 1977. CRC Handbook of Chemistry and Physics. 58th edition. CRC Press, Inc., Cleveland, USA.

APPENDIX: GEOMETRY AND MATERIAL PARAMETERS

A1 General

Table 13: FRAC3DVS input data differing from the Reference Case (see NAGRA, 2002c).

Input	Units	Values	Source/comment
Nuclides and Decays			
Nuclides and decays to be used.	Half lives are specified in years.	Analysed nuclides: organic ^{14}C, ^{36}Cl, ^{41}Ca, ^{79}Se, ^{129}I Half lives from NAGRA (2002c)	
Data for bentonite			
Hydraulic conductivity	m s^{-1}	$1.0 \cdot 10^{-13}$	(NAGRA, 2002c)
Peclet number	dimensionless	dispersion neglected	
Specific storage coefficient	m^{-1}	$2.0 \cdot 10^{-4}$	Based on data reported in (NAGRA, 2002c)
Data for Opalinus Clay			
Thickness of Opalinus Clay	m	80	Extent of model domain (including emplacement tunnel and EDZ)
Peclet number	dimensionless	dispersion neglected	
Retardation	dimensionless	Calculated from the other parameters.	
Specific storage coefficient	m^{-1}	10^{-5}	(NAGRA, 2002c)
Source Term Information			
Source flux	mol s^{-1}	Output from SPENT: Radionuclide release rate from canister to bentonite (Reference Case)	

A2 Geometry

Table 14: Important geometry factors for the Opalinus Clay formation and the repository outline.

Parameter	Unit	Value	Data Source
Thickness of Opalinus Clay formation	m	80	Extent of model domain (including emplacement tunnel and EDZ)
Thickness of „Untere Rahmengesteine“	m	60	(NAGRA, 2002a)
Radius of canister/inner radius of bentonite (spent fuel)	m	0.525	(NAGRA, 2002b)
Outer radius of bentonite/equivalent radius of the converged emplacement tunnels (spent fuel)	m	1.15	(NAGRA, 2002b)
Distance between the centres of the emplacement tunnels (spent fuel)	m	40	(NAGRA, 2002b)
Radius of the converged emplacement tunnels (ILW-1)	m	4.5	(NAGRA, 2002b)
Length of emplacement tunnel (ILW-1)	m	180	(NAGRA, 2002b)

A3 Conversion factors

All FRAC3DVS calculations are done in the kilogram-metre-year system. Hence, all the values for the material parameters given in SI units (kilogram-metre-second) have to be converted into this system.

conversion factor:

1yr = 365.25 days x 24 hrs x 3600 sec =31557600 sec

A4 Opalinus Clay

Table 15: Material parameters directly related to the Opalinus Clay formation.

Parameter	Unit	Value	Data source/remarks
Hydraulic conductivity in vertical direction	$m\ s^{-1}$	$2.0 \cdot 10^{-14}$	(NAGRA, 2002a)
Hydraulic conductivity in horizontal direction	$m\ s^{-1}$	$1.0 \cdot 10^{-13}$	(NAGRA, 2002a)
Flow porosity	-	depends on radionuclide	same as transport porosity (see also NAGRA, 2002c)
Dry bulk density	$kg\ m^{-3}$	$2.43 \cdot 10^{3}$	(NAGRA, 2002a)
Specific storage coefficient	m^{-1}	$1 \cdot 10^{-5}$	(NAGRA, 2002a)

A5 Bentonite filling of the emplacement tunnels

Table 16: Material parameters directly related to the Bentonite filling of the emplacement tunnels.

Parameter	Unit	Value	Data source / Remarks
Hydraulic conductivity	$m\ s^{-1}$	$1.0 \cdot 10^{-13}$	(NAGRA, 2002a)
Flow porosity	-	depends on radionuclide	same as transport porosity (see also NAGRA, 2002c)
Dry bulk density	$kg\ m^{-3}$	$1.77 \cdot 10^{3}$	(NAGRA, 2002a)
Specific storage coefficient	m^{-1}	$2 \cdot 10^{-4}$	(NAGRA, 2002a)

A6 Radionuclides

The effective diffusion coefficient in the different materials is defined in NAGRA (2002a) as $\varepsilon_P \cdot D$, where ε_P is the porosity in the porous material and D is the pore diffusion coefficient. D is different for the Bentonite and the Opalinus Clay. In FRAC3DVS the effective diffusion coefficient in the rock matrix is defined as

$$D_e = \tau \cdot \varepsilon_P \cdot D .$$

Here, only the porosity ε_P changes with the material, the pore diffusion coefficient is assumed to be the same for all materials. For the FRAC3DVS calculations therefore the diffusion coefficient in Bentonite is taken for the whole domain and the tortuosity τ is used as correction factor for the Opalinus Clay subdomain in order to get the effective diffusion coefficients for each material.

Table 17: Material parameters and values used in FRAC3DVS for ^{129}I.

Parameter	Unit	Value	Data source / Remarks
^{129}I Bentonite			
Porosity	-	0.05	(NAGRA, 2002a)
Effective diffusion coefficient in rock matrix	$m^2\ s^{-1}$	$3 \cdot 10^{-12}$	(NAGRA, 2002a)
Distribution coefficient for sorption on rock matrix	$m^3\ kg^{-1}$	$5 \cdot 10^{-4}$	(NAGRA, 2002a)
Half life	a	$1.57 \cdot 10^{7}$	(NAGRA, 2002c)
^{129}I OPA			
Porosity	-	0.06	(NAGRA, 2002a)
Effective diffusion coefficient in rock matrix	$m^2\ s^{-1}$	$1 \cdot 10^{-12}$	(NAGRA, 2002a)
Distribution coefficient for sorption on rock matrix	$m^3\ kg^{-1}$	$3 \cdot 10^{-5}$	(NAGRA, 2002a)
Half life	a	$1.57 \cdot 10^{7}$	(NAGRA, 2002c)
^{129}I input parameters for FRAC3DVS			
Diffusion coefficient	$m^2\ a^{-1}$	$1.89 \cdot 10^{-3}$	
Tortuosity OPA		0.278	
Tortuosity Bentonite		1.0	
Porosity OPA		0.06	
Porosity Bentonite		0.05	
Decay constant	a^{-1}	$4.41 \cdot 10^{-8}$	

Table 18: Material parameters and values used in FRAC3DVS for ^{41}Ca.

Parameter	Unit	Value	Data source / Remarks
^{41}Ca Bentonite			
Porosity	-	0.36	(NAGRA, 2002a)
Effective diffusion coefficient in rock matrix	$m^2\ s^{-1}$	$2 \cdot 10^{-10}$	(NAGRA, 2002a)
Distribution coefficient for sorption on rock matrix	$m^3\ kg^{-1}$	$3 \cdot 10^{-3}$	(NAGRA, 2002a)
Half life	a	$1.03 \cdot 10^{5}$	(NAGRA, 2002c)
^{41}Ca OPA			
Porosity	-	0.12	(NAGRA, 2002a)
Effective diffusion coefficient in rock matrix	$m^2\ s^{-1}$	$1 \cdot 10^{-11}$	(NAGRA, 2002a)
Distribution coefficient for sorption on rock matrix	$m^3\ kg^{-1}$	$1 \cdot 10^{-3}$	(NAGRA, 2002a)
Half life	a	$1.03 \cdot 10^{5}$	(NAGRA, 2002c)
^{41}Ca input parameters for FRAC3DVS			
Diffusion coefficient	$m^2\ a^{-1}$	$1.75 \cdot 10^{-2}$	
Tortuosity OPA		0.15	
Tortuosity Bentonite		1.0	
Porosity OPA		0.12	
Porosity Bentonite		0.36	
Decay constant	a^{-1}	$6.73 \cdot 10^{-6}$	

Table 19: Material parameters and values used in FRAC3DVS for ^{36}Cl.

Parameter	Unit	Value	Data source / Remarks
^{36}Cl Bentonite			
Porosity	-	0.05	(NAGRA, 2002a)
Effective diffusion coefficient in rock matrix	$m^2\ s^{-1}$	$3 \cdot 10^{-12}$	(NAGRA, 2002a)
Distribution coefficient for sorption on rock matrix	$m^3\ kg^{-1}$	0	(NAGRA, 2002a)
Half life	a	$3 \cdot 10^5$	(NAGRA, 2002c)
^{36}Cl OPA			
Porosity	-	0.06	(NAGRA, 2002a)
Effective diffusion coefficient in rock matrix	$m^2\ s^{-1}$	$1 \cdot 10^{-12}$	(NAGRA, 2002a)
Distribution coefficient for sorption on rock matrix	$m^3\ kg^{-1}$	0	(NAGRA, 2002a)
Half life	a	$3 \cdot 10^5$	(NAGRA, 2002c)
^{36}Cl input parameters for FRAC3DVS			
Diffusion coefficient	$m^2\ a^{-1}$	$1.89 \cdot 10^{-3}$	
Tortuosity OPA		0.278	
Tortuosity Bentonite		1.0	
Porosity OPA		0.06	
Porosity Bentonite		0.05	
Decay constant	a^{-1}	$2.31 \cdot 10^{-6}$	

Table 20: Material parameters and values used in FRAC3DVS for ^{79}Se.

Parameter	Unit	Value	Data source / Remarks
^{79}Se Bentonite			
Porosity	-	0.05	(NAGRA, 2002a)
Effective diffusion coefficient in rock matrix	$m^2 s^{-1}$	$3 \cdot 10^{-12}$	(NAGRA, 2002a)
Distribution coefficient for sorption on rock matrix	$m^3 kg^{-1}$	0	(NAGRA, 2002a)
Half life	a	$1.1 \cdot 10^6$	(NAGRA, 2002c)
^{79}Se OPA			
Porosity	-	0.06	(NAGRA, 2002a)
Effective diffusion coefficient in rock matrix	$m^2 s^{-1}$	$1 \cdot 10^{-12}$	(NAGRA, 2002a)
Distribution coefficient for sorption on rock matrix	$m^3 kg^{-1}$	0	(NAGRA, 2002a)
Half life	a	$1.1 \cdot 10^6$	(NAGRA, 2002c)
^{79}Se input parameters for FRAC3DVS			
Diffusion coefficient	$m^2 a^{-1}$	$1.89 \cdot 10^{-3}$	
Tortuosity OPA		0.278	
Tortuosity Bentonite		1.0	
Porosity OPA		0.06	
Porosity Bentonite		0.05	
Decay constant	a^{-1}	$6.3 \cdot 10^{-7}$	

Table 21: Material parameters and values used in FRAC3DVS for $^{14}C_{org}$.

Parameter	Unit	Value	Data source / Remarks
$^{14}C_{org}$ Bentonite			
Porosity	-	0.36	(NAGRA, 2002a)
Effective diffusion coefficient in rock matrix	$m^2\ s^{-1}$	$2 \cdot 10^{-10}$	(NAGRA, 2002a)
Distribution coefficient for sorption on rock matrix	$m^3\ kg^{-1}$	0	(NAGRA, 2002a)
Half life	a	$5.73 \cdot 10^{3}$	(NAGRA, 2002c)
$^{14}C_{org}$ OPA			
Porosity	-	0.12	(NAGRA, 2002a)
Effective diffusion coefficient in rock matrix	$m^2\ s^{-1}$	$1 \cdot 10^{-11}$	(NAGRA, 2002a)
Distribution coefficient for sorption on rock matrix	$m^3\ kg^{-1}$	0	(NAGRA, 2002a)
Half life	a	$5.73 \cdot 10^{3}$	(NAGRA, 2002c)
$^{14}C_{org}$ input parameters for FRAC3DVS			
Diffusion coefficient	$m^2\ a^{-1}$	$1.75 \cdot 10^{-2}$	
Tortuosity OPA		0.15	
Tortuosity Bentonite		1.0	
Porosity OPA		0.12	
Porosity Bentonite		0.36	
Decay constant	a^{-1}	$1.21 \cdot 10^{-4}$	

A7 Boundary conditions

Table 22: Parameters related to the boundary conditions.

Parameter	Unit	Value	Data source / Remarks
Hydraulic gradient in OPA	m m^{-1}	1	(NAGRA, 2002a)
Concentrations at geosphere boundaries	mol m^{-3}	0	(NAGRA, 2002a), see also Figure 5; top boundary: Wedelsandstein W, bottom boundary: Sandsteinkeuper Sk; W and Sk are assumed to act as „fast“ sinks and are implemented as zero concentration boundaries
Mass flow at near field/canister boundary	mol a^{-1}		Output from SPENT: Radionuclide release rate from canister to bentonite (Reference Case)

Table 23: Hydraulic and transport boundary conditions for boundaries A-F (see Figure 8).

Parameter	Unit	Value	Data source / Remarks
Hydraulic head at boundary A	m	0	For consolidation enhanced transport see Table 25
Concentration at boundary A	mol m^{-3}	0	Zero concentration boundary
Hydraulic head at boundary B	m	depends on gradient and model dimensions	For consolidation enhanced transport see Table 25
Concentration at boundary B	mol m^{-3}	0	Zero concentration boundary
Boundary C			No-flow boundary for both, flow and transport
Boundary D			No-flow boundary for both, flow and transport
Boundary E			No-flow boundary for both, flow and transport
Mass flow at boundary F	mol a^{-1}	depends on nuclide	Output from SPENT: Radionuclide release rate from canister to bentonite (Reference Case)

A8 Consolidation enhanced transport

Table 24: Geometry and material parameters related to models which describe consolidation enhanced transport.

Parameter	Unit	Value	Data source / Remarks
Change in hydraulic head (change in overburden)	m	see Table 25	(NAGRA; 2002a, 2002c)
Specific storage coefficient	m^{-1}	depends on material	(NAGRA, 2002a)
Gravitational acceleration	ms^{-2}	9.81	WEAST (1977), Table F-179
Density of water	kg m^{-3}	$1.0 \cdot 10^3$	WEAST (1977), Table F-11; for pure water, free from air, for a temperature of 3.98 ℃, Decreases to $0.996 \cdot 10^3$ Kg m^{-3} for a temperature of 30 ℃
Density of ice	Kg m^{-3}	$0.917 \cdot 10^3$	Needed for the calculation of hydraulic heads induced by glacial overburden, from WEAST (1977), table F-1

For the calculation of the pressure increase due to the ice cover, the density of the ice is needed. The value given in Table 24 is a value for gas-free pure water and this is also the highest possible value for the ice density. Ice densities at the top of the glaciers are in general much lower and increase with depth up to 830 – 917 kg m^{-3} (see Table 2.1. in PATERSON, 1994). The value used for the calculation of the pressure increase is therefore a conservative estimate used to calculate the (maximum) pressure increase caused by the ice cover.

Table 25: Glaciation Periods and associated changes of the hydraulic boundary conditions in FRAC3DVS.

start of period [years]	**end of period [years]**	**glacial overburden (ice thickness at surface) [m]**	**hydraulic head at boundary A [m]**	**hydraulic head at boundary B [m]**
0	50000	0	0	160
50000	70000	200	-183.4	-23.4
70000	150000	0	0	160
150000	170000	200	-183.4	-23.4
170000	250000	0	0	160
250000	270000	200	-183.4	-23.4
270000	350000	0	0	160
350000	370000	400	-366.8	-206.8
370000	450000	0	0	160
450000	470000	200	-183.4	-23.4
470000	550000	0	0	160
550000	570000	200	-183.4	-23.4
570000	650000	0	0	160
650000	670000	200	-183.4	-23.4
670000	750000	0	0	160
750000	770000	200	-183.4	-23.4
770000	850000	0	0	160
850000	870000	200	-183.4	-23.4
870000	950000	0	0	160
950000	970000	400	-366.8	-206.8
970000	1000000	0	0	160